Spring 4-17-2017

Relationship Between Structure and Functional Connectivity Within the Default Mode Network

Andrei A. Vakhtin
University of New Mexico - Main Campus

Andrei A. Vakhtin

Candidate

Psychology

Department

This dissertation is approved, and it is acceptable in quality and form for publication:

Approved by the Dissertation Committee:

Claudia D. Tesche, Ph.D. , Chairperson

James F. Cavanagh, Ph.D.

Derek A. Hamilton, Ph.D.

Robert J. Thoma, Ph.D.

RELATIONSHIP BETWEEN STRUCTURE AND FUNCTIONAL CONNECTIVITY WITHIN THE DEFAULT MODE NETWORK

By

ANDREI A. VAKHTIN

M.S., Psychology; University of New Mexico, 2015

B.S., Biology; University of New Mexico, 2009

B.S., Psychology; University of New Mexico, 2009

DISSERTATION

Submitted in Partial Fulfillment of the Requirements for the Degree of

Doctor of Philosophy in Psychology

The University of New Mexico

Albuquerque, New Mexico

May, 2017

ACKNOWLEDGMENTS

I would like to thank my family for providing me with the opportunity to pursue my interests, supporting me throughout my triumphs and failures, and always valuing education above all. I am privileged and thankful to have had the opportunity to work with my advisor Dr. Claudia Tesche, who challenged me in my work and studies, and provided input of tremendous value throughout my endeavors during my graduate academic career. I extend my gratitude to my dissertation committee members Dr. James Cavanagh, Dr. Derek Hamilton, and Dr. Robert Thoma (listed alphabetically) for their time and guidance throughout the project. In addition, I thank Dr. Rex Jung for kindly letting me use the data that are presented in this dissertation, as well as all supporting lab members who helped collect them.

RELATIONSHIP BETWEEN STRUCTURE AND FUNCTIONAL CONNECTIVITY WITHIN THE DEFAULT MODE NETWORK

By

ANDREI A. VAKHTIN

B.S., Biology, University of New Mexico, 2009

B.S., Psychology, University of New Mexico, 2009

M.S., Psychology, University of New Mexico, 2015

Ph.D., Psychology, University of New Mexico, 2017

ABSTRACT

We proposed a novel measure of conceptualizing dynamic functional network connectivity (FNC) in the human brain using flexibility of functional connectivity (fFC), which captures the variance of functional connectivity across time. In task-free fMRI scans (N = 122), this measure was demonstrated to correspond to the underlying structural connectivity (SC) within the default mode network (DMN), while static functional connectivity (sFC) did so to a relatively low degree. As SC likely does not develop to facilitate task-free brain function, but rather to integrate information during cognitive engagement, we argue that fFC can estimate the potential functional connectivity exhibited outside of the task-free setting to a greater degree than sFC, and is better suited for examining behavioral correlates of FNC. In support of this, we showed that SC-fFC coupling was related to intelligence levels, while SC-sFC coupling was not. Further, we found that the DMN existed in a functionally disconnected state during a large

portion of the scan, raising questions about whether sFC is a meaningful quantifier of functional connectivity in the absence of a task, and scrutinizing its extrapolative power to real-world, cognitively engaging scenarios. Given that fFC is based on FNC variability across time rather than its average, it is largely unaffected by such contaminants.

TABLE OF CONTENTS

LIST OF FIGURES

LIST OF TABLES

GLOSSARY OF ACRONYMS

ACC – Anterior Cingulate Cortex

DMN – Default Mode Network

DTI – Diffusion Tensor Imaging

ICA – Independent Component Analysis

FC – Functional Connectivity

fFC – Flexibility of Functional Connectivity

fMRI – Functional Magnetic Resonance Imaging

l-AG – Left Angular Gyrus

MFG – Middle Frontal Gyrus

PCA – Principal Component Analysis

PCC – Posterior Cingulate Cortex

Prec – Precuneus

r-AG – Right Angular Gyrus

r-MTG – Right Middle Temporal Gyrus

ROI – Region of Interest

SC – Structural Connectivity

sFC – Static Functional Connectivity

sFC(dir) – Directional Static Functional Connectivity

sFC(mag) – Magnitude of Static Functional Connectivity

SFG – Superior Frontal Gyrus

CHAPTER 1: INTRODUCTION

Background and Specific Aims

In trying to understand how brain activity is related to behavior and cognition, traditional neuroimaging data analyses have been focused on isolating brain regions that become "active" during the performance of experimental tasks. However, analyses focusing on regionally or temporally constrained aspects of function have limitations in advancing our understanding of the brain as a complex and dynamic system, no single part of which functions in a truly independent fashion. The knowledge base regarding functional and structural hierarchies of brain organization has grown tremendously over the past decade (Sporns et al. 2004; van den Heuvel and Hulshoff Pol 2010), in large part due to the potential realized in network-based approaches, particularly as applied to task-free scans.

Task-free neuroimaging data are collected while the subject lies in the scanner and thinks of nothing in particular, staring at a cross on the screen or with eyes closed. As the brain is never "off," the ongoing fluctuations of brain activity levels in the absence of task engagement are of particular interest, given their potential to reveal robust baseline functional processes that are not task-specific and may serve as markers of neurological and psychiatric disorders. Conventional event-related analyses are not applicable to functional neuroimaging data that are not task-driven due to the lack of *a priori* temporal information that is needed for relating brain activity to behavior. Brain function in a task-free setting is not random, however, and has consistently been

demonstrated to exhibit highly organized inter-regional patterns of connectivity (Fox et al. 2005). The first such network was observed in fMRI data as a correlation between cross-hemispheric blood oxygenation level-dependent (BOLD) signals in the bilateral motor cortices (Biswal et al. 1995). Subsequent investigations of whole-brain connectivity patterns have shown that brain activity can be represented in terms of multiple spatially distributed networks that display high levels of intrinsic coherences and possess unique time courses.

Particularly advantageous is the fact that such functional networks can be extracted by examining the spatiotemporal structures of functional data in the absence of tasks or other *a priori* information. Although several different well-described network extraction techniques exist, all ultimately aim to reduce high-dimensional neuroimaging data to several components, each one of which may involve several brain regions that work in synchrony. While such networks are defined by the high levels of intrinsic coherences that exist within them, they also display varying levels of weaker correlations between each other. Over the past several years, the number of analyses examining functional network connectivity (FNC) interactions has ballooned into a formidable sub-field of neuroscience, which has subsequently revolutionized our conception of the brain as a dynamic, hierarchical system of systems.

A major challenge to reliable quantification of FNC measures and interpretation of any FNC relations to behavioral processes is the lack of knowledge about the structural and functional influences that generate, maintain, and guide FNC. Motivated by previous publications describing positive

relationships between functional connectivity and structure across regions that were pre-defined anatomically (Hagmann et al. 2008; Skudlarski et al. 2008; Honey et al. 2009), we examined the structure-function relationship across regions that were defined functionally. Specifically, we extracted functional networks within the broader default mode network from task-free scans, and examined the association between their underlying structural connections and inter-network functional connectivity (FC) levels. Further, we proposed a novel conceptualization of inter-network functional interactions by examining the variances that pairs of networks exhibit in their FC levels across time, and investigated the relationship between this FC measure and structure. The motivation behind the use of FC variances instead of averages was to circumvent addressing negative and positive FC between network pairs in relating them to structure. Finally, we examined the relationships between different types of structure-function coupling with individual differences in general cognitive ability.

Default Mode Network

The default mode network (DMN; Raichle et al. 2001) has been consistently shown to display prominent, intrinsically coherent activity in the absence of task engagement, and has received a great deal of attention following the inception of network-based analyses. Its name stems from its propensity to become active during a lack of cognitive engagement, as we dwell in a default state of cognition. Interestingly, the DMN exhibits decreased levels of activity during task engagement (Shulman et al. 1997; Mazoyer et al. 2001). The network

is broadly distributed across the cortex, and occupies the bilateral angular gyri, precuneus, medial and lateral prefrontal cortex, as well as the posterior cingulate cortices – regions that display synchronous activities, as detected by various neuroimaging modalities such as fMRI BOLD (Van Dijk et al. 2010), PET (Raichle et al. 2001), EEG (Fomina et al. 2015; Knyazev et al. 2016), and MEG (Brookes et al. 2011).

While much research has focused on determining the functional role of the DMN, its exact purpose remains unknown. Generally, the network appears to be related to cognition regarding the self, including assessment of stimulus self-relevance in both non-social (Qin et al. 2016) and social situations (Lee 2015; Soch et al. 2016). More interestingly, the network has been implicated in mind-wandering about past or hypothetical future events (Karapanagiotidis et al. 2016; Kucyi et al. 2016), something that most healthy humans engage in without external preoccupation. Specifically, future planning and assessment regarding personal goals has been demonstrated to rely on the DMN (Xu et al. 2016). Although such self-reflective and long-term planning processes have long been considered to be strictly human attributes, the DMN has recently been described in other non-primate animals, such as dogs (Kyathanahally et al. 2015; Robinson et al. 2016) and rodents (2012; Gozzi and Schwarz 2016) – findings that challenge our previous conceptions of animal cognition and the purpose of the DMN in humans.

Given the wide scope and demanding nature of the supposed DMN roles – as it must rapidly respond to the ever-changing shifts in cognitive demands and

constantly evaluate situational self-relevance – the functional spectrum that this network is capable of occupying would be expected to be broad. Indeed, the range of its connectivity potential to other networks is unusually high, with the DMN shifting from being highly synchronous with a particular network at one point in time, yet becoming nearly perfectly anti-correlated with it at another instance within the same scan. Recent findings further demonstrated the existence of smaller networks within the larger DMN, which in turn display functional heterogeneity within the DMN itself (Chen et al. 2017). In light of the high level of functional variance the DMN is capable of exhibiting, we focused on such within-DMN networks, and examined the structure-function relationship across their pairs.

Greicius et al. (2009) have previously demonstrated that FC within the DMN system does indeed reflect the structural connectivity (SC) that underlies it. The DMN is a particularly suitable candidate for considerations of such SC-FC relationships, as non-human primate anatomical studies have demonstrated that many of the within-DMN structural connections are monosynaptic (Lavenex et al. 2002; Kobayashi and Amaral 2003; Mantini et al. 2011), mitigating the fact that SC analyses focused on direct connections between a pair of networks may miss intermediate connections (*i.e.,* via a third region). Additionally, non-human primates have been shown to display FC during task-free scans that reflected SC even in the case of multi-synaptic paths within the DMN (Mantini et al. 2011). While the potential of such a relationship is promising and exciting, the (Greicius et al. 2009) human study utilized static functional connectivity (see section 6.2),

which is blind to fluctuations that network pairs inevitably exhibit in their connectivity strengths across time. Further, the functional network extraction method used to isolate the DMN was seed-based, which, while able to reveal spatially separate regions of the network, may fail to capture sub-components that are functionally distinct (Joel et al. 2011). In other words, the lack of a constraint upon which spatially separate DMN sub-components are isolated misses the system's functional architecture, and, by extension, could result in decreased white matter tract specificities if these sub-components were used as regions of interest (ROIs) for structural tractography. In light of the potential structure-function relationship that has previously been described within the DMN system, the present study applies an advanced network extraction method called independent component analysis (ICA), which imposes maximal statistical independence onto the extracted functional networks within the DMN.

Network Extraction Using Independent Component Analysis

Independent component analysis is a blind source separation algorithm that is used to find statistically independent information (Delorme et al. 2007) based on non-Gaussianity. It does so by estimating the components that linearly mix to form the observed signal (Jutten and Herault 1991; Comon 1994). An *m* x *t* matrix X of observed neuroimaging data across *m* locations and *t* time points can therefore be defined as

$$X = AS,$$

where S is an *n* x *t* matrix containing *n* components' true source data, and A is a static *m* x *n* mixing weights matrix that linearly combines source data S to form the observed signal X. With only X being known, both A and S are undetermined, and need to be estimated by ICA. This is achieved by learning weights in the un-mixing matrix A^{-1}, the inverse of A, such that when combined with the observed signal X, features of S are maximally mutually independent. Accordingly, the equation above can therefore be rearranged as:

$$XA^{-1} = S .$$

Prior to ICA decomposition, data are commonly preprocessed using principal component analysis (PCA), which imposes statistical de-correlation onto the data up to the second statistical moment (Xi et al. 2000). Independent component analysis (ICA) then extracts networks from PCA-whitened data based on third or fourth order moments, depending on the algorithm used. Given that ICA operates on skewedness and kurtosis, however, it would be no more useful than PCA in separating two Gaussian components from their joint distribution (Dodel et al. 2000).

The fMRI community has extensively utilized ICA in investigating functional brain networks. Given that fMRI offers more information in the spatial domain of the data, variants of spatial ICA are commonly used for network extraction. In selecting the ICA algorithm, the expected source distributions need to be considered, with fMRI sources of interest tending to be non-Gaussian. More specifically, focal fMRI activations have been shown to have super-Gaussian distributions, while artifact-related sources are often sub-Gaussian (McKeown

and Sejnowski 1998; Calhoun and Adali 2006). This discrepancy presents challenges for ICA algorithms that are partial to isolating sub- or super-Gaussian sources, as the former would produce a set of nuisance components, while the latter may yield cognition-related components that are contaminated with noise.

An algorithm capable of dissociating components with low and high kurtoses is therefore desirable for fMRI decomposition, with the extended Infomax ICA fitting this criterion. Although Infomax is more computationally demanding than FastICA, this burden is negligible in practice due to the relatively small amount of fMRI data that is usually analyzed, at least in comparison to EEG/MEG. Indeed, both simulation and real fMRI examinations have shown extended Infomax outperforming algorithms like FastICA and JADE in both the estimation of true sources (Correa et al. 2005) and reliability across multiple runs (Correa et al. 2007). Importantly, combinations of preprocessing steps involving PCA, clustering, and various ICA types have also been contrasted, showing that PCA coupled with spatial extended Infomax yielded the best results (Calhoun et al. 2001).

Structural Inter-Network Connectivity

Structural connectivity analyses commonly operate on data obtained using diffusion weighted imaging (DWI), which measures diffusivity of water molecules in the brain (Douek et al. 1991). Given that neuronal axons, which congregate to form large white matter fiber bundles that connect spatially separated brain regions, are filled with fluid, Brownian motion of water within them is restricted by

their cell membranes and would be expected to display movement biased along the direction of the axon. Diffusion weighted imaging (DWI) is an MRI technique that can be used to detect the vector of such Brownian motion, producing images with intensities that reflect diffusion magnitudes (Stejskal and Tanner 1965). Specifically, the application of a diffusion-encoding gradient that is perpendicular to the diffusion direction results in highest intensity, while gradients applied in the direction of the neuronal axons are least sensitive to their water movement. Using a scan sequence that utilizes 3 orthogonal gradients therefore allows for the estimation of directionality within each voxel, producing isotropic (a. k. a. trace) DWI diffusion maps.

In order to track specific fiber bundles through the brain, however, one can utilize diffusion tensor (DTI) fitted data to determine the principal diffusion directions within a three-dimensional tensor ellipsoid within each voxel, which theoretically requires diagonalizing diffusion coefficients obtained from nine gradient-encoding directions (D_{xx}, D_{xy}, D_{xz}; D_{yx}, D_{yy}, D_{yz}; D_{zx}, D_{zy}, D_{zz}). However, in practice determining the principal diffusion directions of the tensor ellipsoid only necessitates a minimum of 6 gradient direction due to the redundancy between $D_{xy} = D_{yx}$, $D_{yz} = D_{zy}$, and $D_{xz} = D_{zx}$. The process of fitting tensors *via* diagonalization of multi-gradient data thus provides direction and magnitude of water diffusion within each voxel, allowing for applications of tractography methods to tensor data.

Application of tractorgraphy to DTI data allows for detection of large white matter bundles between spatially separate ROIs. A number of fiber-tracking

algorithms exist, falling into broad categories of deterministic and probabilistic tractography techniques. Deterministic methods are concerned with estimating the most likely direction of the tract that traverses each location, reconstructing a single bundle that exists between seed ROIs by either fitting a uniform fiber direction within each voxel (Mori et al. 1999), tensorline (Weinstein et al. 1999), or interpolation methods. A major limitation of deterministic approaches is the assumption that only one tract passes through each voxel. Given that voxel size is much larger than individual neuronal axons, this assumption may be violated as multiple tracts may pass through a particular voxel in different directions. Probabilistic tractography techniques allow for modeling multiple directions of diffusion at each location across the entire distance between ROIs, selecting the most probable total path after voxel-wise estimations. Given that probabilistic tractography takes into account data from all of the voxels' diffusion estimates across the entire path between ROIs, the method tends to reconstruct tracts with a greater degree of fidelity than deterministic techniques. A specific probabilistic white matter tracking method utilized in the present study was the multi-fiber field model (Behrens et al. 2007), applied using Functional MRI of the Brain (FMRIB) Software Library (FSL), which yields a count of streamlines that likely pass through each voxel, as well as a number of streamlines that have satisfied all tractography conditions (*i.e.* "made it" from seed to target ROI).

Static Functional Inter-Network Connectivity

While brain networks exhibit strong within-network connectivity levels, as this is the main criterion on which they are derived, relatively weak associations also exist between different network time courses. This functional network connectivity can be obtained between every pair of networks extracted from a particular dataset, producing a network-pairwise connectivity matrix. The resulting holistic representation of each network's propensity to communicate with every other network paints a useful picture of large-scale cognitive systems that supposedly function in synchrony, as well as those operating non-reciprocally.

Pearson *r* correlation is the most common method to assess FC between a pair of networks. Correlating two time courses across the entire time of the scan results in a single connectivity value for each pair of networks. A given dataset decomposed into *n* networks, therefore, can be summarized as a collection of *n*-choose-two *r* values. While these whole-scan correlations shed light on interesting relationships between various cognitive sub-systems, such as the default-mode network's tendency to display activity that is generally anti-correlated with the rest of the brain, the usefulness of inferences made from static long-term network interactions is beginning to fade. This is largely a product of the consensus that the brain does not exist in a temporally-stable state of connectivity, but rather exhibits dynamic, transient patterns of network interactions (Sporns et al. 2004).

In the investigation described herein, we included two measures of static functional connectivity (sFC): raw directional sFC (sFC(dir)) that included the sign of the SC-sFC relationship, and the magnitude of sFC (sFC(mag)) that was obtained by taking the absolute value of directional FC within each network pair and subject. The latter approach was taken in an attempt to address anti-correlations that some network pairs were likely to exhibit.

Flexibility of Functional Inter-Network Connectivity

Changes in network connectivity strengths can be examined using dynamic functional network connectivity. This is achieved by calculating bivariate connectivity measures, such as Pearson *r*, between a pair of networks' time courses across multiple windows that are shifted across scan time. Conducting such an analysis on a single pair of networks would produce a time course of connectivity strength between them, which in turn can be used as an experimental measure of interest. Much like any other signal, a connectivity time course for a particular network pair can be analyzed simply in terms of variables such a amplitude and variance, for example (Allen et al. 2012).

A much more interesting approach considers a collection of such connectivity time courses between every possible combination of network pairs of interest in a particular dataset. Using methods such as k-means clustering, congregations of such time courses can be separated into several connectivity matrices that collectively explain a large portion of total connectivity variance, yet represent separate states of connectivity that are quasi-stable and reoccur

across time, existing for different durations that are referred to as dwell times. In other words, if one were to take a holistic connectivity snapshot of the brain at a random time point, she or he will likely find the brain in one of such states of connectivity. Connectivity states thus summarize the centroids of dynamic functional connectivity via several connectivity matrices that collectively reflect the single connectivity matrix obtained via static FC analyses.

Here, we used the variance of the connectivity strengths distributed across such centroids for a given pair of networks within the DMN system to determine the pair's flexibility of functional connectivity (fFC). The use of fFC as a measure of interest rather than static FC is motivated by the difficulties involved in a bivariate analysis between the always-positive SC and FC that can be both positive and negative. For a given network pair, we operationally define its fFC as the standard deviation of the FC strengths it displays across the different FC states across the duration of the scan.

Hypotheses

Our expectation for the relationship between structure and static connectivity between functionally defined networks was reflective of the previously described positive SC-sFC correlations between anatomically defined regions of interest: we expected SC to be positively correlated with sFC(dir) and sFC(mag). Further, we hypothesized that stronger structural connectivity between DMN networks would be associated with greater fFC as well. Specifically, DMN networks with stronger structural connections between them

were expected to exhibit higher standard deviations of FC across different functional states.

CHAPTER 2: METHODS

Participants and Behavioral Measures

One hundred twenty two volunteer participants were recruited via flyers from the University of New Mexico in Albuquerque and surrounding areas. The University's institutional review board approved the study protocol in accordance with the ethics principles set by the Declaration of Helsinki. Subjects were presented with a consent form and given an opportunity to ask an investigator questions pertaining to the study prior to providing consent. Legal guardians signed approved assent forms for participants who were under the age of 18 years old.

All individuals subsequently underwent intelligence testing by a trained investigator using the Wechsler Abbreviated Scale of Intelligence-II (WASI-II) battery. Specifically, vocabulary, block design, similarities, and matrix reasoning tests we used to estimate general intelligence levels.

fMRI Collection and Preprocessing

Functional MRI scans were collected at the Mind Research Network, Albuquerque, NM, using a 3-Tesla Siemens Trio Tim MRI system. Functional T_2^*-weighted scans were obtained via a 32-channel radio frequency coil using an echo-planar imaging (EPI) of 32 ascending interleaved slices with the following

parameters: TR = 275 ms, TE = 30 ms, flip angle = 34^{o}, slice thickness = 3.5 mm, distance factor = 33%, FOV = 240 mm, voxel size = 3.8 x 3.8 x 3.5 mm^3. A total of 1352 EPI volumes were collected during each of the task-free scans, during which participants were instructed to look at the crosshairs in the middle of the screen in front of them and think of nothing in particular. Structural T1 volumes were reconstructed from 192 multi-echo MPRAGE slices obtained with the following parameters: TR = 2530 ms, TE = 1.64/3.5/5.36/7.22/9.08 ms, voxel size = 1 x 1 x 1 mm^3, FOV = 256 mm.

The first 22 fMRI scans were discarded from each subject's dataset in order to remove volumes with magnetic saturation effects. Preprocessing of the functional data was done using Statistical Parametric Mapping (SPM) 12 toolbox and custom MATLAB scripts. Following the conversion of DICOM files to NIfTI format, all volumes were corrected for slice timing effects. Volumes collected across time were then re-aligned to the first image within each subject, and a single mean image with spatial orientation representing the entire scan was produced for each participant. These subject-specific average volumes were subsequently co-registered to the corresponding individual structural T1 anatomy volumes, and the resulting spatial transformation matrices applied to all 1330 EPI volumes, aligning every person's functional and structural data in space. Next, each individual's T1 scan was normalized to the Montreal Neurological Institute (MNI) template using the tissue probability maps provided with the SPM toolbox. Individual T1-to-MNI spatial transformation matrices were then applied to all EPI volumes from each participant, producing functional data residing in common

MNI space for further group statistics. Lastly, all functional data were smoothed using a 6 mm kernel.

fMRI Network Extraction and ROI Definition

With the aim of obtaining multiple DMN networks that can be used to examine within-DMN structural and functional connectivity, we used a high-order fMRI decomposition model. Using the Group ICA of fMRI Toolbox (GIFT; http://mialab.mrn.org/software/gift), fMRI data were first whitened using expectation maximization principle component analysis (PCA) and reduced to 100 principal components. The extended Infomax spatial ICA algorithm was subsequently utilized to reduce the aggregate data to 100 independent components with maximal statistical independence.

Default-mode networks were identified in the resulting set of components by examining their spatial distributions and matching them with previously described DMN components. Specifically, Pearson *r* spatial correlation strengths between the *t*-maps of the obtained components and those described in Allen et al. 2012 were computed. Those with *r* values of 0.5 or higher were deemed as candidates for a match, and underwent further visual examinations to confirm positive identifications. As a safeguard against admitting artifact-related components into the final dataset, as well as to resolve ambiguities in the case of multiple components representing previously-described ones, low:high frequency signal ratios displayed by component activity histograms were also considered.

Components with high low:high frequency ratios were favored for positive identification, as low ratios are indicative of system noise (Allen et al. 2011).

Once the DMN networks were identified, we thresholded them at the 80th percentile of their respective *t* distributions to define regions of interest (ROIs) for white matter tractography. The threshold was chosen with the goal of avoiding spatial overlap between ROIs, as well as capturing the centroids that contain most of the voxels that functionally contribute to their respective networks. Further, the produced ROIs were checked to ensure that they, while residing in the gray matter, did spatially protrude into the white matter for tractography purposes.

With the ROIs defined in standard MNI template space, we then spatially transformed them to each participant's native space. This was achieved by co-registering the MNI template to the native volumes, and applying the resulting transformation matrices to the entire set of DMN ROIs. Within each subject, voxel coordinates of ROIs' maximum values were then used to calculate the Euclidean distances, in millimeters, between every possible pair of networks. This produced 122 subject-specific sets of inter-network distances that would be used as covariates to account for morphological variations, as well as examine any effects distance may have on structural and functional connectivity levels. Likewise, subject-specific ROI volumes, in voxels, were obtained for SC normalization further in the analysis.

Structural Connectivity

Diffusion weighted imaging (DWI) data were obtained on the same Siemens Trio scanner and visit as the functional and structural scans. The following parameters were used to obtain the EPI images: TR = 3600 ms, TE = 110 ms, voxel size = 2.2 x 2.2 x 2.2 mm^3, 66 slices, FOV = 229 mm, 150 diffusion directions with b = 1000–3000 s/mm^2, 6 measurements with b = 0. Diffusion-weighted scans were preprocessed using FSL. Following susceptibility artifact correction by removing the difference between diffusion weights obtained via scans in ascending and descending slice order, the data were further corrected for eddy currents. The diffusion tensor model was then fit to each subject's data, and Bayesian estimation of diffusion parameters obtained using sampling techniques while modeling crossing fibers (BEDPOSTX; (Behrens et al. 2007)) was run on individual subjects' data in native space.

Regions of interest that were previously derived from functional networks were spatially transformed to every subject's native space, and input as seeds and target regions into the probabilistic tracking function (PROBTRACKX2), which utilized bi-directional tracking algorithms. Each voxel within the seed mask emanated 5000 sample streamlines, and allowed for a maximum voxel-to-voxel streamline curvature of approximately 80 degrees. The built-in "loopcheck" option was used to exclude pathways that looped back onto themselves. The output of the tractography algorithm included the number of pathways that had satisfied the user-specified tracking conditions, and successfully spanned the space between the seed and target masks. This value was normalized by dividing it by

the total number of streamlines that were sampled out of each ROI, producing a fraction that represented the tracking “success rate” between each network pair. Given the positively-skewed distribution of the obtained fraction values, a log transform was applied to the produced structural connectivity data.

Static Functional Connectivity and Flexibility of Functional Connectivity

In order to account for scanner drift, linear, quadratic, and cubic trends were removed from the identified DMN networks’ time courses. The time courses were de-spiked and low-pass filtered using a 1.25 Hz upper frequency limit, yielding a signal with a bandwidth that is conservative for fMRI data with a repetition time of 0.275 s, as per Nyquist-Shannon sampling theorem (Shannon 1949). Temporal derivatives of subject-specific scan-to-scan x, y, and z translations as well as roll, pitch, and yaw motion parameters were regressed out of the networks’ time courses. Finally, time courses were normalized using variance normalization. For each subject, static functional connectivity (sFC) levels were obtained via Pearson *r* correlations between whole-scan time courses of network pairs.

Dynamic connectivity time courses were obtained by calculating covariance matrices within a time window with a width of 22 TR (6.05 s) and a 3 TR Gaussian taper (0.825 s) that slid across time in increments of 1 TR, producing pairwise network connectivity time courses with 1308 time points each. Using the GIFT dynamic functional connectivity toolbox, functional connectivity states among the DMN networks were then isolated by applying the k-means

clustering algorithm (Lloyd 1982) to the covariance matrices calculated for each window in the previous step. Rather than the Euclidean distance function (L2), the L1 norm was used as a similarity measure due to its increased effectiveness in high dimensional data (Aggarwal et al. 2001). We did not explicitly specify the number of clusters to be isolated, instead relying on the built-in gap and silhouette statistics cluster estimations, and using the average of the two as the final number of connectivity states to be estimated. Following cluster identification, the network pairs' correlational strengths within each FC state were Fisher z-transformed in order to obtain normalized sets of recurring functional connectivity levels among DMN network pairs.

Following the cluster analysis of ICA-derived functional networks' time courses, individual subjects' contributions to the group FC states were used to derive subject-specific FC matrices for every state. For every participant, the amounts of time that she or he spent in each FC state were then used to weight that subject's corresponding FC states' levels. This was achieved by dividing the number of time points spent in a state by the number of time windows sampled across the entire scan session (1308), and multiplying the result by every FC value in that particular state. Weighing FC states by dwell times thus incorporated the variability in FC state occurrences and dwell times across subjects, producing subject-wise values for every network-pair that represent the pairs' general propensities to communicate. While the resulting scalars no longer represented true correlational FC values, they prevented subjects who reached certain states rarely and for short periods of time from over-contributing to our

main measure of interest – the flexibility of functional connectivity – defined as the standard deviation of these values for each network pair across all FC states. The fFC was calculated in this manner for every network pair on a subject-wise basis.

Effects of Distance on Connectivity

We first examined the potential effects of inter-network distances on connectivity levels. Pearson *r* correlations between inter-network distance and structural connectivity, static functional connectivity, and flexibility of functional connectivity were calculated within each subject. The three resulting vectors of *r* values for the entire group were Fisher z transformed and entered into one-sample *t* tests to obtain summary statistics for the relationships between distance and each type of connectivity. Similarly, separate summary statistics for the male and female groups were also calculated. Further, individual z values from the male and female groups were entered into two-sample *t* tests to examine gender differences in distance-connectivity relationships. Correlations between group-averaged distances and levels of SC, sFC, and fFC were also obtained for the entire group, as well as males and females separately. Although the analysis cannot provide insight into individual within-subject relationships between distance and connectivity, we included it to examine the general sample-wide relationships of whether distance affects connectivity on average.

Relationship Between Structural and Functional Connectivity

The relationship between structural and static functional connectivity levels was assessed across all network pairs within each subject via partial correlations, adjusted for inter-network distances. The relationship was examined in two analogous analyses using raw directional sFC(dir) as well as sFC(mag), which was obtained by taking the absolute value of raw sFC values. The two approaches were taken in an attempt to account for competing fundamental assumptions of how SC may relate to sFC(dir). Specifically, it is yet to be clarified whether anti-correlations and positive synchronies that exist between functional networks are influenced by SC in the same manner. Linear relationships between sFC(dir) and structure imply that positive and negative functional connections depend on SC in an inverse fashion. That is, higher SC is related to stronger FC in networks that exhibit positive synchronies, yet results in weaker FC in anti-correlated network pairs. Using sFC(mag) conversely assumes that the increased structural connections would be associated with higher levels of functional connectivity regardless of FC direction, in both positively and anti-correlated network pairs. This discrepancy has been subjected to extensive discussion, and is a major motivator for the main aim of this study to consider the flexibility of dynamic network interactions in lieu of static directional FC measures.

Partial SC-sFC(dir), SC-sFC(mag), and SC-fFC correlations, adjusted for inter-network distances, were calculated among the identified DMN networks within each subject. The resulting individual *r* values were Fisher z transformed

and entered into three separate one-sample *t* tests in order to determine whether the group-level SC-sFC(dir), SC-sFC(mag), SC-fFC correlations significantly deviated from zero. A repeated measures analysis of variance (ANOVA) was used to assess the differences between the means of the three types of SC-FC coupling (SC-sFC(dir), SC-sFC(mag), and SC-fFC). A multivariate analysis of variance was utilized to assess the effects of gender, age, and IQ on each type of SC-FC coupling (SC-sFC(dir), SC-sFC(mag), SC-fFC).

CHAPTER 3: RESULTS

Demographics and Behavioral Measures

The distribution of participants' ages displayed a positive skew and the variable was log transformed for all subsequent parametric statistical tests (Figure 1). The group mean age was 21.7 +/- 3.5 y. o. (57 males = 21.5 +/- 3.6 y. o., 65 females = 21.8 +/- 3.4 y. o.). The age difference between genders was not statistically significant ($t(120) = 0.5724$, $p = 0.5681$). Intelligence levels, as estimated via the WASI-II test, were normally distributed, with the whole group mean of 112 +/- 11 (57 males = 111 +/- 11, 65 females = 112 +/- 12; Figure 2). No significant difference in IQ levels between genders was detected ($t(120) = 0.4186$, $p = 0.6763$). We note that the estimated intelligence levels in the described sample were nearly a whole standard deviation above the population mean of 100, which is an expected finding given that the majority of participants were university students.

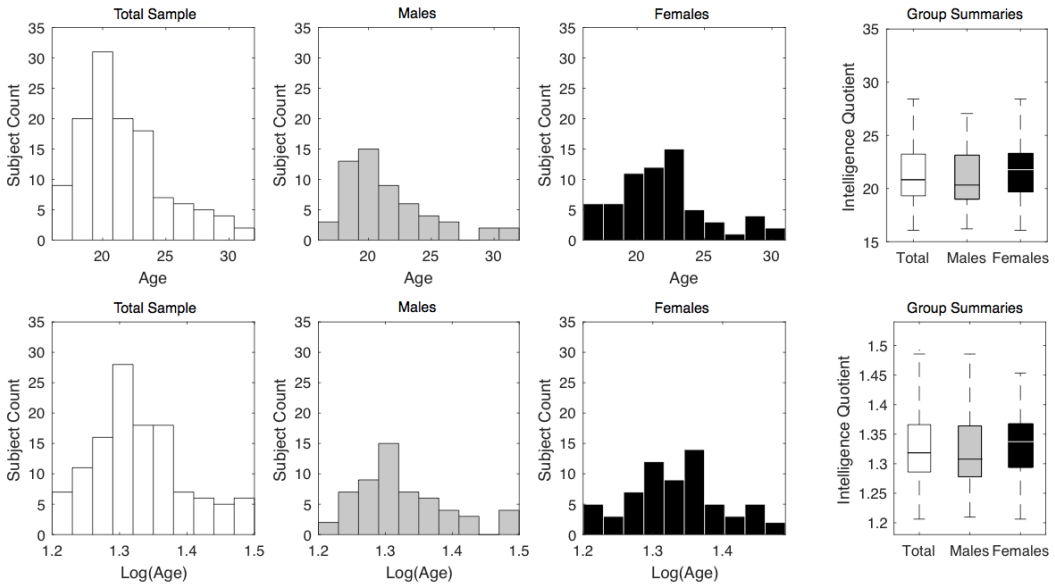

Figure 1. Age Summary. Distributions of age are shown for the entire study sample (N = 122), the male group (n = 57), and the female group (n = 65). The age variable displayed a positive skew (top panel) and was log-transformed (bottom panel) prior to being subjected to parametric statistical tests further in the analysis pipeline. A two-sample *t*-test revealed no statistical age difference between genders ($t(120) = 0.5724$, $p = 0.5681$).

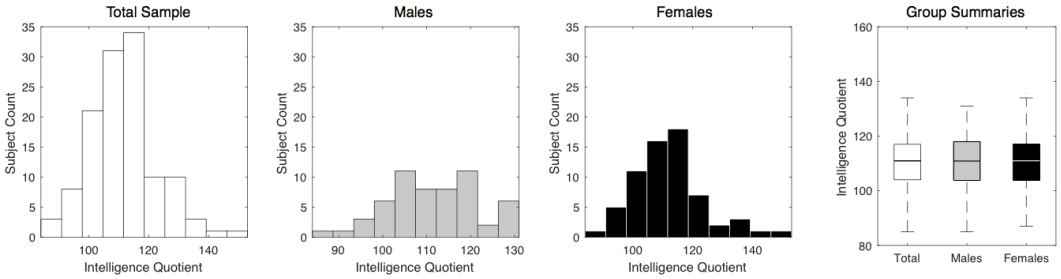

Figure 2. Intelligence Levels Summary. Distributions of intelligence quotient (IQ) are presented for the entire study sample (N = 122), the male group (n = 57), and the female group (n = 65). The difference between genders in terms of IQ was not statistically significant ($t(120) = 0.4186$, $p = 0.6763$).

ICA Decomposition and Region of Interest Creation

The ICA decomposition of group aggregate fMRI data yielded 100 independent components. Out of the resulting dataset, we identified 9 networks deemed to belong to the DMN. The selected networks were named according to the anatomical regions that their centroids occupied: anterior cingulate cortex (ACC), left angular gyrus (l-AG), middle frontal gyrus (MFG), posterior cingulate

cortex (PCC), inferior precuneus (prec1), superior precuneus (prec2), right angular gyrus (r-AG), right middle temporal gyrus (r-MTG), and superior frontal gyrus (SFG). The networks' *t* distribution maps were thresholded at the 80th percentile to create ROIs suitable for tractography, and are presented in Figure 3. Network volumes spanned a wide range and were therefore used for normalization of the subsequent tractography analyses (Figure 4). We note that these values should not be interpreted as anatomical volumetric measures of the described regions. While functional network nomenclature used herein is based on the regions that the networks centroids occupied, some networks did protrude beyond the borders of the anatomical structures that they were named after. Network distances displayed a normal distribution suitable for parametric tests, and are shown in Figure 5.

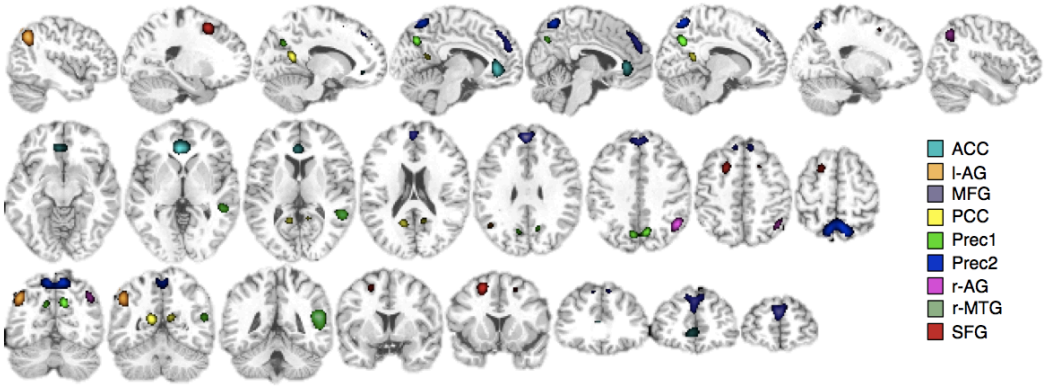

Figure 3. Default Mode Networks. Examined default mode system networks shown in representative slices. The spatial distributions of the DMN networks are presented in different colors. Nine networks within the default mode network were selected out of the 100 components produced by independent component analysis. Each network's *t* distribution was thresholded at the 80th percentile (shown) in order to create non-overlapping ROIs for white matter tractography that also encompass the functional networks' centroids. ACC – anterior cingulate cortex, l-AG – left angular gyrus, MFG – middle frontal gyrus, PCC – posterior cingulate cortex, prec1 – precuneus, prec2 – precuneus, r-AG – right angular gyrus, r-MTG – right middle temporal gyrus, SFG – superior frontal gyrus.

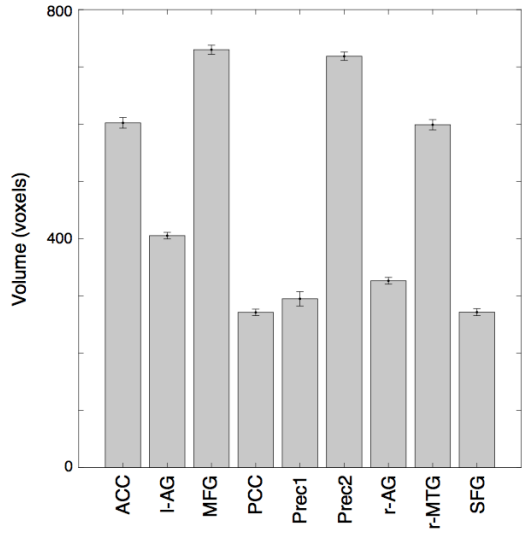

Figure 4. Volumes of Regions of Interest (ROIs). ACC – anterior cingulate cortex, l-AG – left angular gyrus, MFG – middle frontal gyrus, PCC – posterior cingulate cortex, prec1 – precuneus, prec2 – precuneus, r-AG – right angular gyrus, r-MTG – right middle temporal gyrus, SFG – superior frontal gyrus.

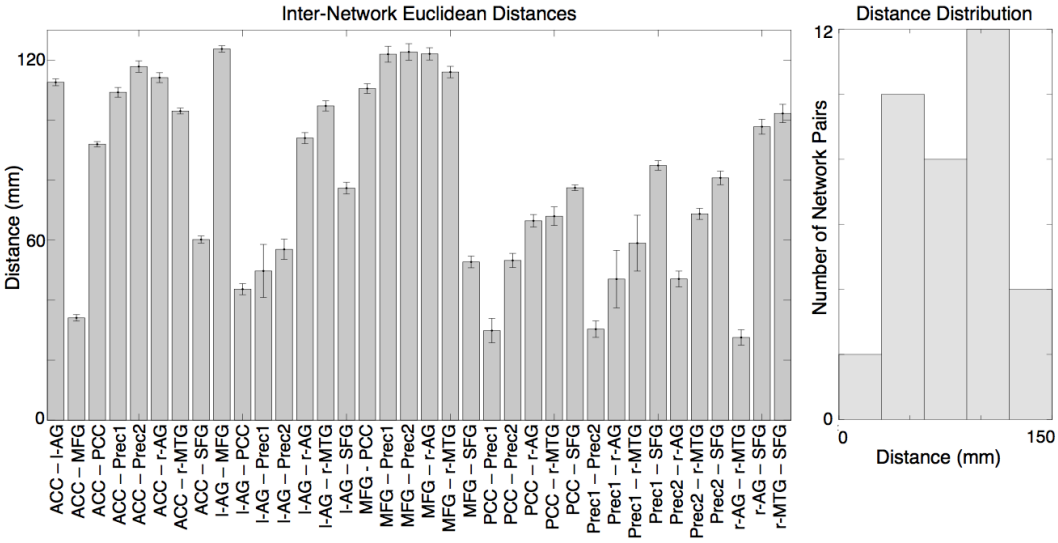

Figure 5. Inter-Network Distances. Euclidean distances between maximum voxels of functional network pairs are presented. Inter-ROI distances averaged across subjects are presented in millimeters for the whole study sample (N = 122). The histogram on the right shows the distribution of inter-network distances, which was normal. ACC – anterior cingulate cortex, l-AG – left angular gyrus, MFG – middle frontal gyrus, PCC – posterior cingulate cortex, prec1 – precuneus, prec2 – precuneus, r-AG – right angular gyrus, r-MTG – right middle temporal gyrus, SFG – superior frontal gyrus.

Connectivity Measures

The raw streamline counts that were successful in connecting the seed networks to the target networks are presented in Figure 6. The fractions of successful streamlines out of the total number sampled displayed a positive skew, and were therefore log transformed. The resulting distribution is shown in Figure 6. Although cross-hemispheric connections to the angular gyri were successfully detected in these 150-directional scans, the SC strengths in these network pairs did display elevated levels of variance across subjects. Such findings are likely linked to the previously described challenges in tracking inter-parietal fibers that encounter the corona radiata and the superior longitudinal fasciculus on the way. Even with the powerful imaging methodology employed herein, the trackability of such white matter pathways thus remains a concern.

Static directional functional connectivity levels are presented in Figure 7. Averaged sFC(dir) levels were largely positive, with only four network pairs (ACC – Prec2, l-AG – Prec2, MFG – Prec1, MGF – Prec2) displaying anti-correlations across the entire scan. Magnitudes of sFC across network pairs are shown in Figure 8. Both sFC(dir) and sFC(mag) measures were normally distributed. While we intended to additionally examine the SC-FC relationship in anti-correlated and positively correlated networks separately, the analysis proved to be unfeasible due to the low number of anti-correlated networks in the data.

Dynamic functional connectivity time courses were separated into six clusters, as suggested by the gap and silhouette estimations. The resulting FC states are presented in Figures 9-14. State 4 was the most prevalent across the

entire scan time, with participants spending nearly half of the time in this FC state. Of interest is that this particular state did not involve high levels of connectivity between any network-pairs, and can be described as a state of general disconnectedness. Conversely, state 6 was characterized by relatively high positive connectivity levels among all network pairs. Other states involved variable mixtures of both anti-correlated and positively correlated inter-network interactions. Although most of the time was spent in state 4, the remaining states were reached at similar rates, with subjects spending around 10% of the scan session in each one. The standard deviations of the dwell time-weighted correlations in each FC state, which represent our operational definition of FC flexibility, are presented in Figure 15. The obtained fFC values were normally distributed.

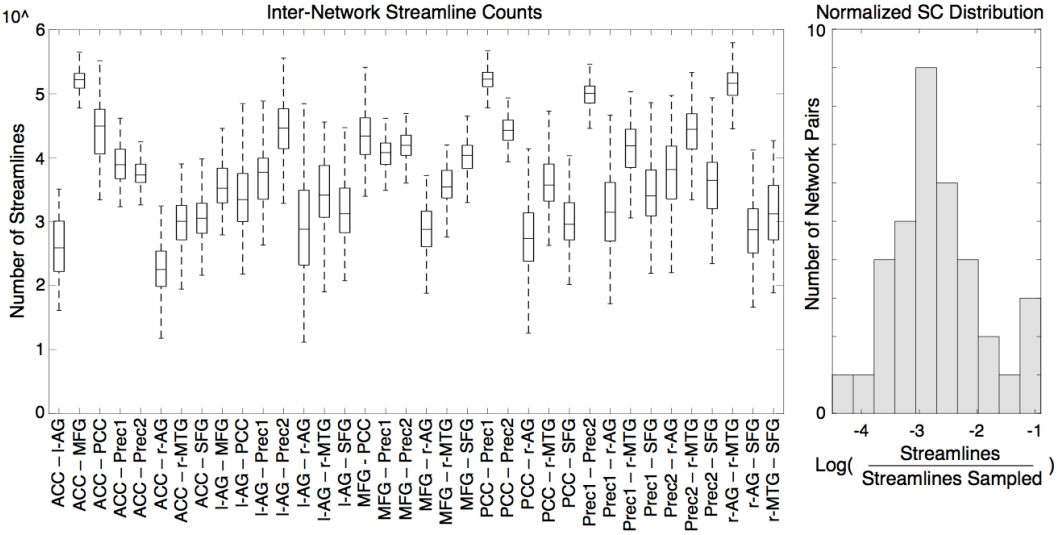

Figure 6. Summary of Structural Connectivity. The box plot on the left summarizes group streamline counts that satisfied inter-network tractography conditions. Raw streamline counts were log-scaled for illustration purposes. For normalization, raw streamline counts were divided by the number of total streamlines sampled from each network seed, producing fractions of streamlines that succeeded in reaching their respective target masks. These streamline fractions were further log-transformed in order to get rid of the positive skew. The histogram on the right shows the distribution of normalized structural connectivity measures averaged across subjects. ACC – anterior cingulate cortex, l-AG – left angular gyrus, MFG – middle frontal gyrus, PCC – posterior cingulate cortex, prec1 – precuneus, prec2 – precuneus, r-AG – right angular gyrus, r-MTG – right middle temporal gyrus, SFG – superior frontal gyrus.

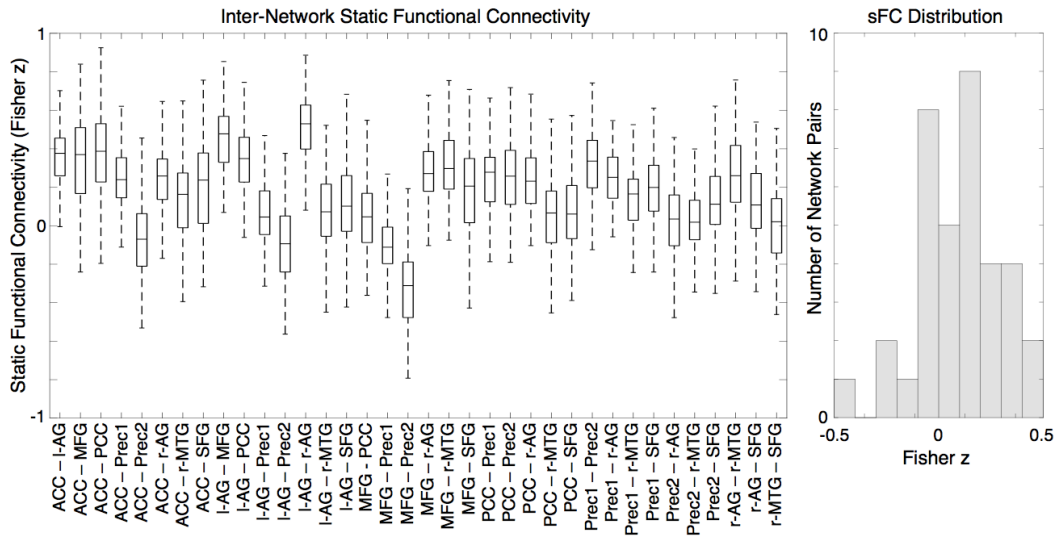

Figure 7. Directional Static Functional Connectivity. Levels of directional static functional connectivity (sFC(dir)) are summarized for each pair of DMN networks via box plots. The histogram shows the distribution of sFC(dir) levels averaged across subjects. ACC – anterior cingulate cortex, l-AG – left angular gyrus, MFG – middle frontal gyrus, PCC – posterior cingulate cortex, prec1 – precuneus, prec2 – precuneus, r-AG – right angular gyrus, r-MTG – right middle temporal gyrus, SFG – superior frontal gyrus.

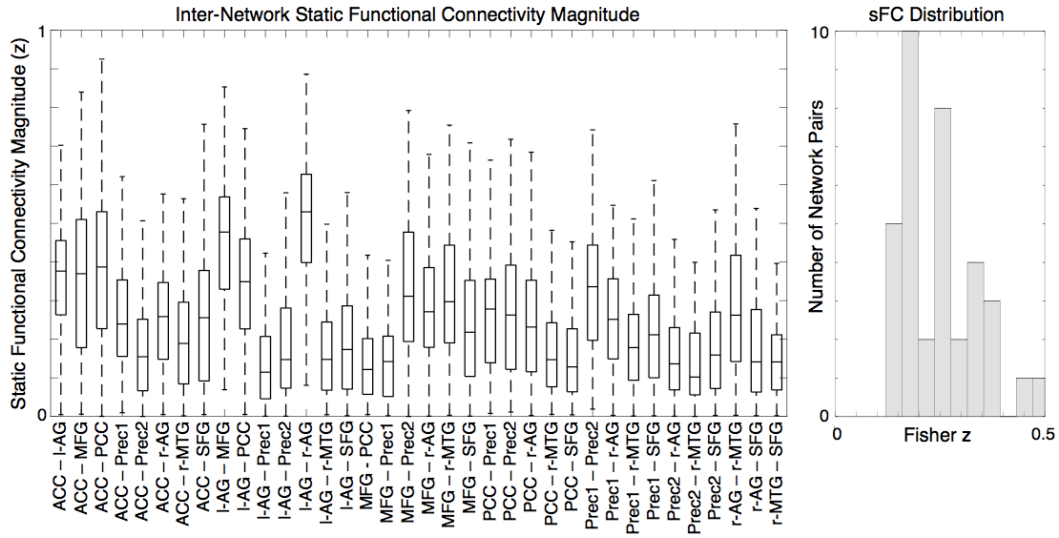

Figure 8. Magnitude of Static Functional Connectivity. Levels of static functional connectivity magnitude (sFC(mag)) are summarized for each pair of DMN networks via box plots. The histogram shows the distribution of sFC magnitudes averaged across subjects. ACC – anterior cingulate cortex, l-AG – left angular gyrus, MFG – middle frontal gyrus, PCC – posterior cingulate cortex, prec1 – precuneus, prec2 – precuneus, r-AG – right angular gyrus, r-MTG – right middle temporal gyrus, SFG – superior frontal gyrus.

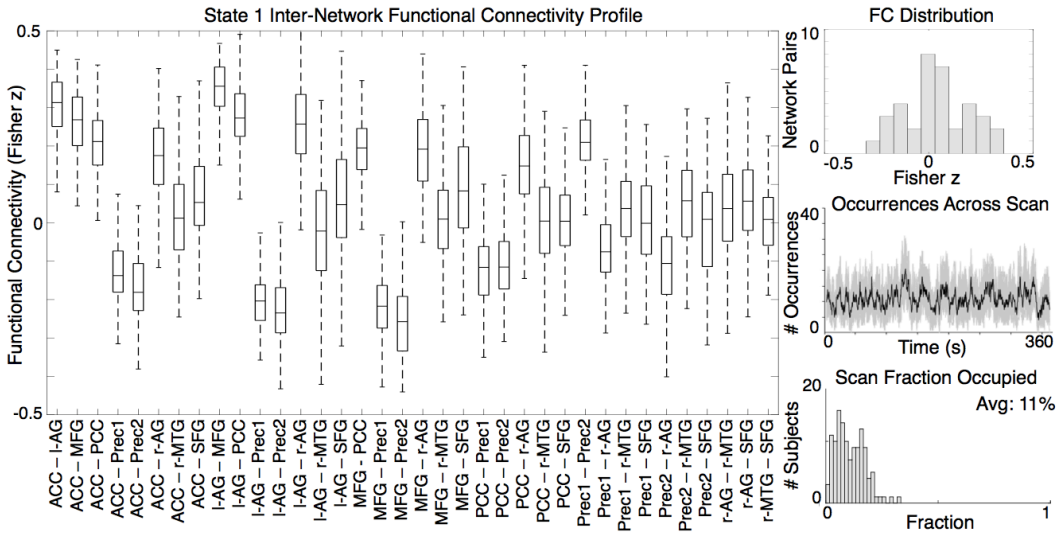

Figure 9. Summary of Functional Connectivity State 1. The box plot presents group FC levels during the state in each network pair. The distribution of FC levels is shown in the histogram in the top right panel. The number of occurrences that the state exhibited in the entire group throughout the scan session is presented in the middle-right panel. The bottom-right histogram summarizes the number of subjects who spent various amounts of time in this state as a fraction of the entire scan session. The average percentage of the scan session that the entire group spent in this state is also presented.

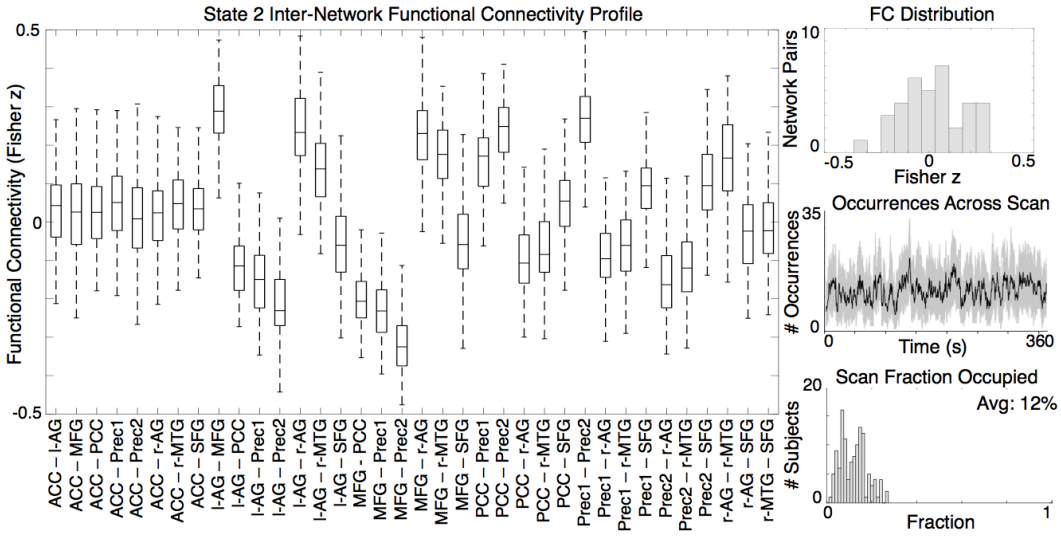

Figure 10. Summary of Functional Connectivity State 2. The box plot presents group FC levels during the state in each network pair. The distribution of FC levels is shown in the histogram in the top right panel. The number of occurrences that the state exhibited in the entire group throughout the scan session is presented in the middle-right panel. The bottom-right histogram summarizes the number of subjects who spent various amounts of time in this state as a fraction of the entire scan session. The average percentage of the scan session that the entire group spent in this state is also presented.

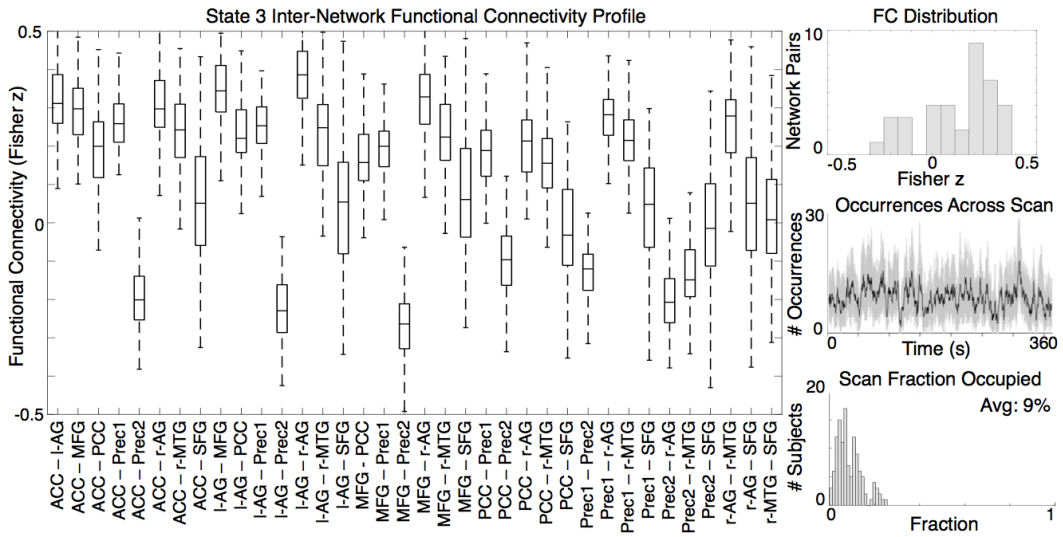

Figure 11. Summary of Functional Connectivity State 3. The box plot presents group FC levels during the state in each network pair. The distribution of FC levels is shown in the histogram in the top right panel. The number of occurrences that the state exhibited in the entire group throughout the scan session is presented in the middle-right panel. The bottom-right histogram summarizes the number of subjects who spent various amounts of time in this state as a fraction of the entire scan session. The average percentage of the scan session that the entire group spent in this state is also presented.

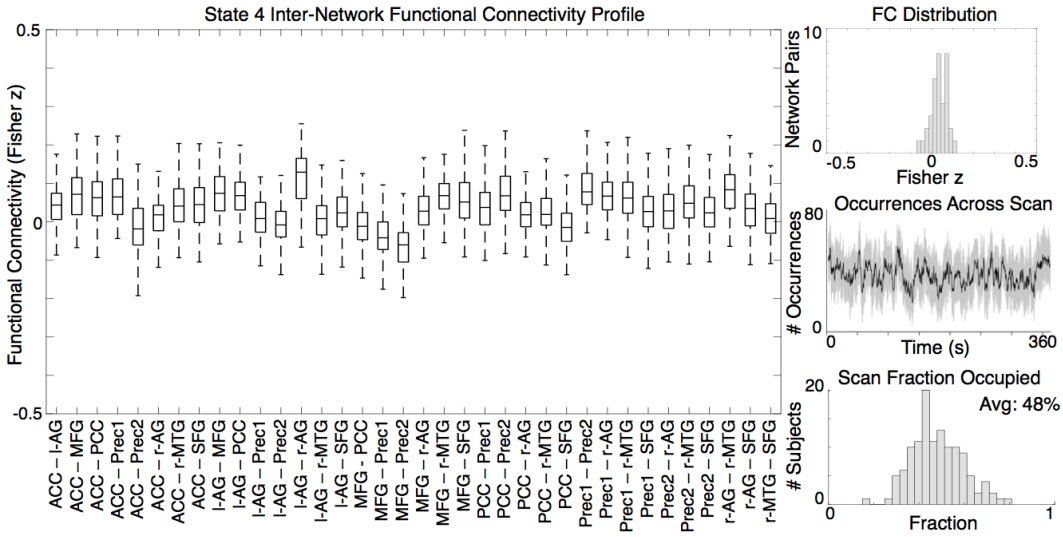

Figure 12. Summary of Functional Connectivity State 4. The box plot presents group FC levels during the state in each network pair. The distribution of FC levels is shown in the histogram in the top right panel. The number of occurrences that the state exhibited in the entire group throughout the scan session is presented in the middle-right panel. The bottom-right histogram summarizes the number of subjects who spent various amounts of time in this state as a fraction of the entire scan session. The average percentage of the scan session that the entire group spent in this state is also presented.

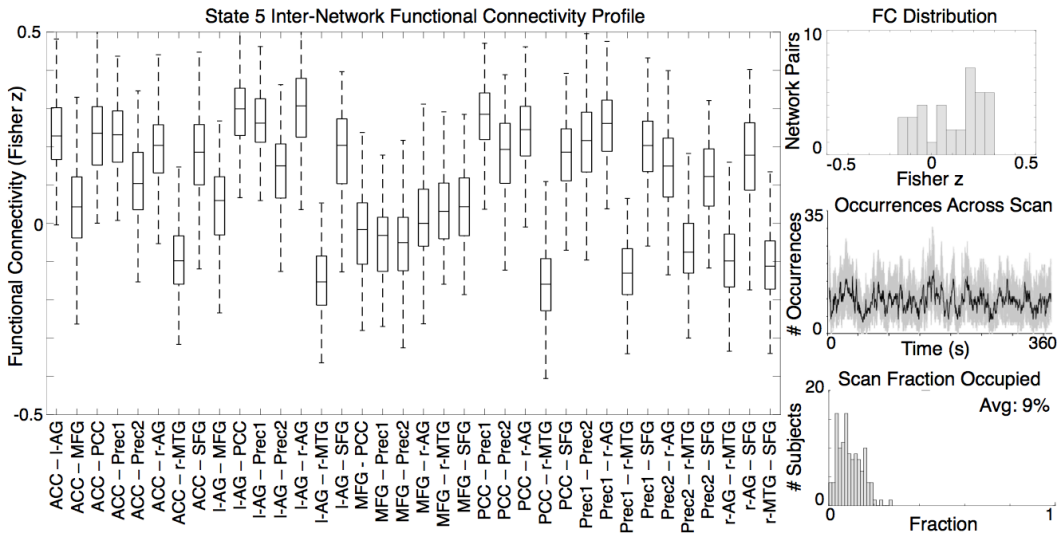

Figure 13. Summary of Functional Connectivity State 5. The box plot presents group FC levels during the state in each network pair. The distribution of FC levels is shown in the histogram in the top right panel. The number of occurrences that the state exhibited in the entire group throughout the scan session is presented in the middle-right panel. The bottom-right histogram summarizes the number of subjects who spent various amounts of time in this state as a fraction of the entire scan session. The average percentage of the scan session that the entire group spent in this state is also presented.

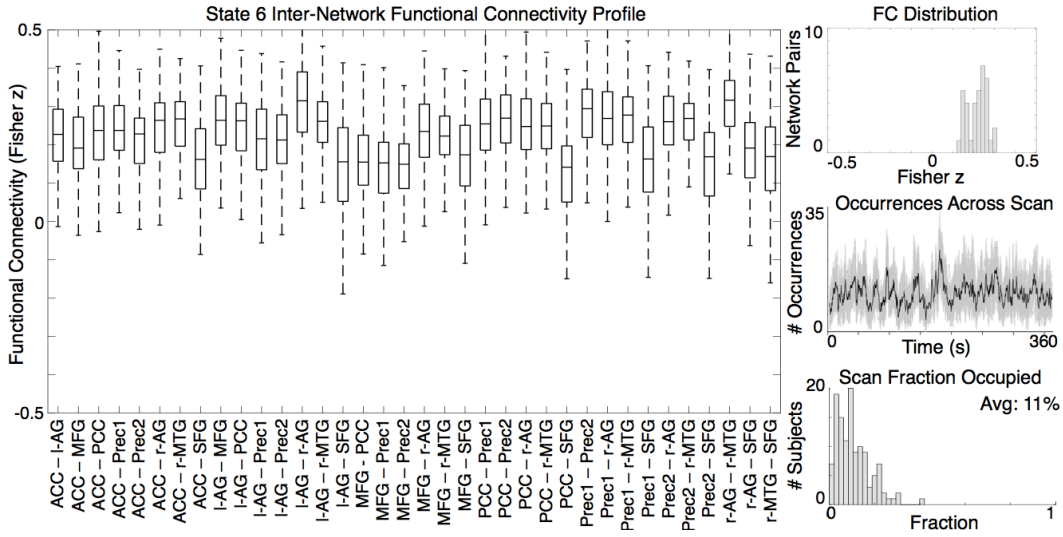

Figure 14. Summary of Functional Connectivity State 6. The box plot presents group FC levels during the state in each network pair. The distribution of FC levels is shown in the histogram in the top right panel. The number of occurrences that the state exhibited in the entire group throughout the scan session is presented in the middle-right panel. The bottom-right histogram summarizes the number of subjects who spent various amounts of time in this state as a fraction of the entire scan session. The average percentage of the scan session that the entire group spent in this state is also presented.

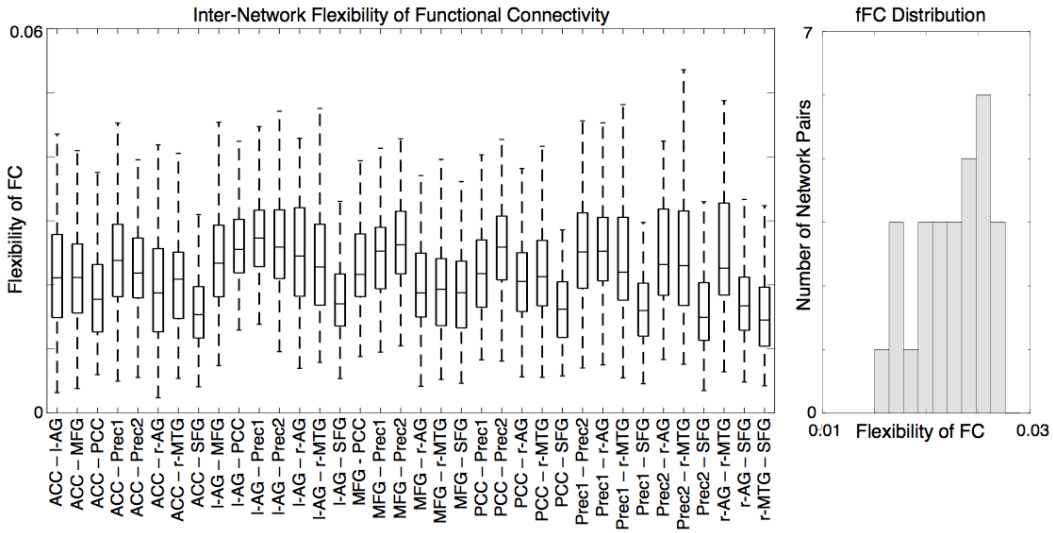

Figure 15. Flexibility of Functional Connectivity. The box plot presents the flexibilities of functional connectivity for each network pair. For every subject, fFC was obtained by weighting the network pairs' functional connectivity values within each state by that state's dwell time, and taking the standard deviation of the resulting values across all states for each network pair separately.

Connectivity and Distance

The relationship between SC and inter-network distance was homogeneously negative across the entire study group (Figure 16). All subjects displayed diminishing SC levels with increased distance ($t(121) = -49.4263$, $p < 0.001$). The relationship between sFC(dir) and distance was overwhelmingly negative across the study sample, with increased inter-network distances associated with lower sFC(dir) (Figure 17). The majority of subjects displayed strong negative correlations between the two measures, but weaker positive associations were detected in several participants. The summary statistic for the distance-sFC(dir) relationship was statistically significant for the entire group ($t(121) = -9.5644$, $p < 0.001$). The magnitude of static FC (Figure 18) was not significantly correlated with distance ($t(121) = 1.8258$, $p = 0.0703$). Finally, distance and fFC (Figure 19) were significantly negatively correlated within the

entire cohort ($t(121) = -7.2673$, $p < 0.001$). While correlations of averages do not capture within-subject variances and should generally not be utilized for inferring relationships between the measures of interest on a subject level, we conducted such analyses for population-level demonstrative purposes. On average, increases in inter-network distances did predict lower levels of SC in the whole group ($r(34) = -0.5833$, $p < 0.001$). However, average distance was not predictive of average sFC(dir) ($r(34) = -0.1759$, $p = 0.3049$) or sFC(mag) ($r(34) = 0.0544$, $p = 0.7525$). Further, correlations of averaged inter-network distances and averaged fFC failed to reach statistical significance as well ($r(34) = -0.2560$, $p = 0.1319$).

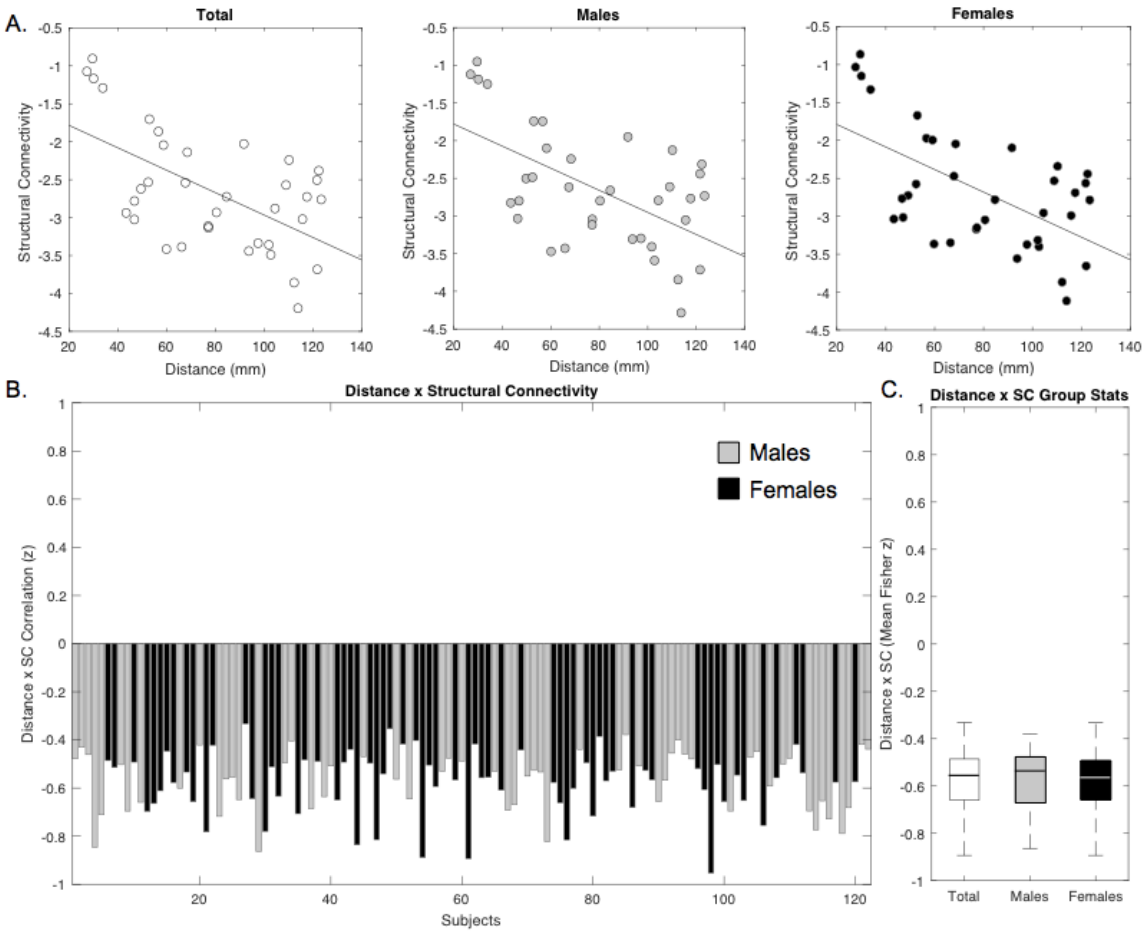

Figure 16. Relationship Between Inter-Network Distances and Structural Connectivity Levels. A. Correlations of distance and SC averages across subjects are shown for 36 pairs of DMN networks for the whole group ($r(34) = -0.5833$, $p < 0.001$), as well as for the 57 males and the 65 females separately. B. Individual within-subject correlations between distance and SC using 36 pairs of DMN networks are shown. Correlation strengths are presented as Fisher-transformed z values. C. The box plots summarize the distributions of the within-subject correlations between distance and SC for the whole group, the male group, and the female group. A one sample t-test was used to compute the summary statistic of the distance-SC relationships for the whole group ($t(121) = -49.4263$, $p < 0.001$).

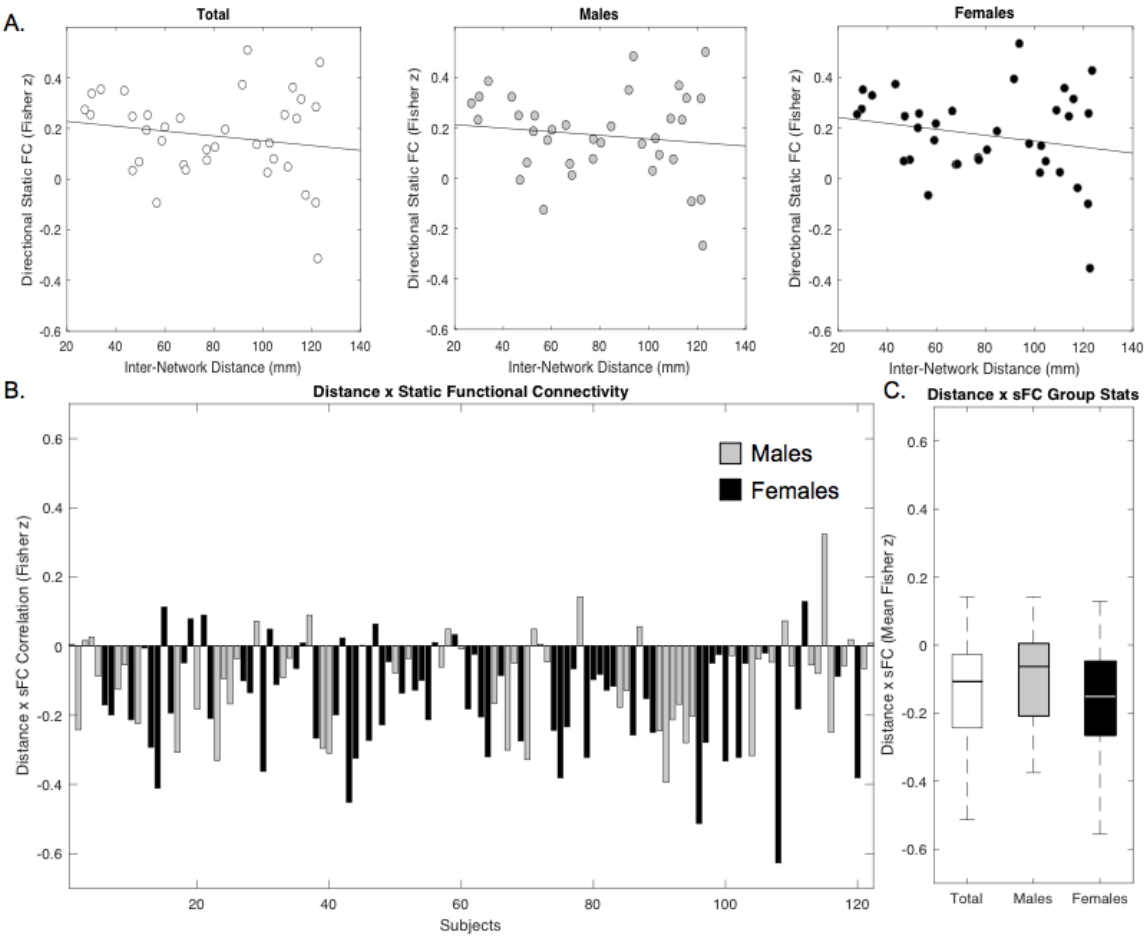

Figure 17. Relationship Between Inter-Network Distance and Directional Static Functional Connectivity. A. Correlations of distance and sFC(dir) averages across subjects are shown for 36 pairs of DMN networks for the whole group ($r(34) = -0.1759$, $p = 0.3049$), the 57 males, and the 65 females. B. Individual within-subject correlations between distance and sFC(dir) using 36 pairs of DMN networks are shown. Correlation strengths are presented as Fisher-transformed *z* values. C. The box plots summarize the distributions of the within-subject correlations between distance and sFC for the whole group, the male group, and the female group. A one sample *t*-test was used to compute the summary statistic of the distance-sFC(dir) relationship for the whole group ($t(121) = -9.5644$, $p < 0.001$).

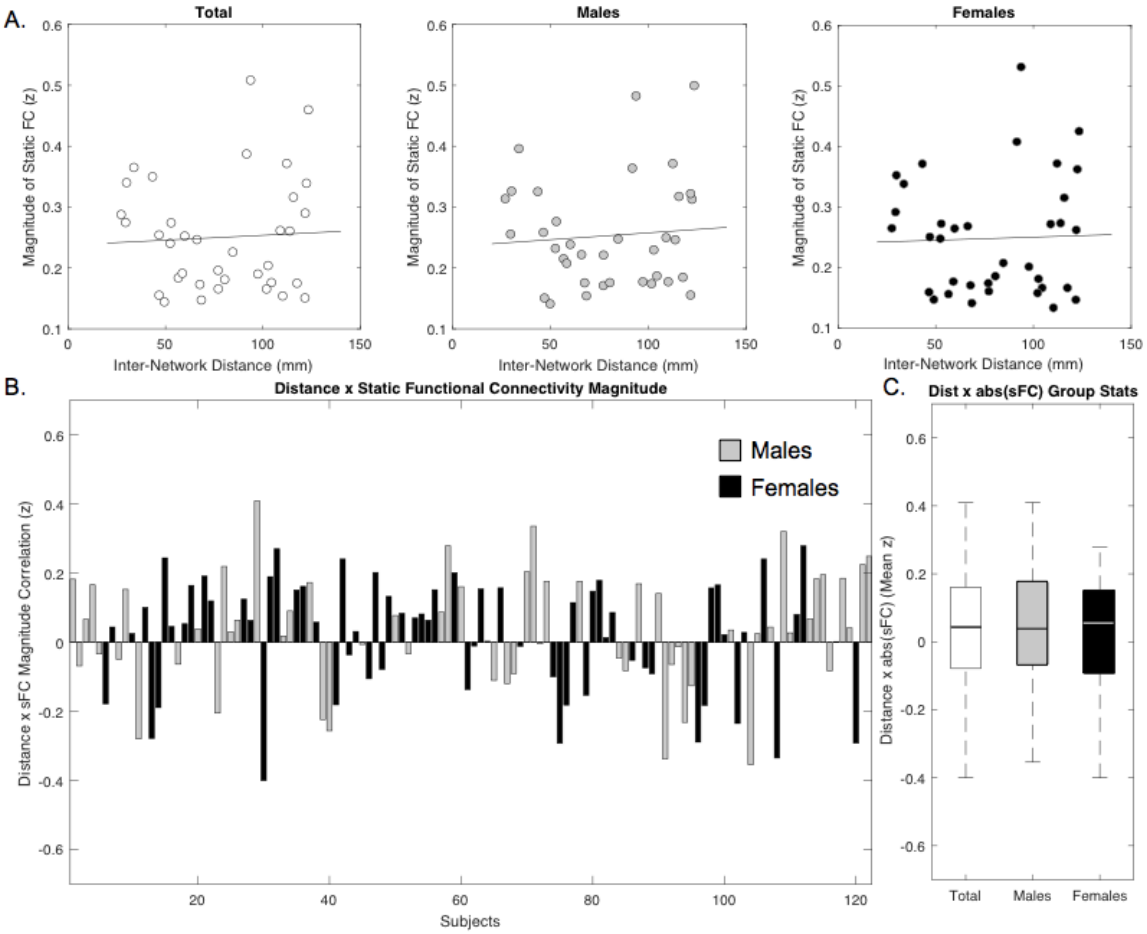

Figure 18. Relationship Between Inter-Network Distance and the Magnitude of Static Functional Connectivity. A. Correlations of distance and sFC(mag) averages across subjects are shown for 36 pairs of DMN networks for the whole group ($r(34) = 0.0544$, $p = 0.7525$), the 57 males, and the 65 females. B. Individual within-subject correlations between distance and sFC(mag) using 36 pairs of DMN networks are shown. Correlation strengths are presented as Fisher-transformed *z* values. C. The box plots summarize the distributions of the within-subject correlations between distance and sFC(mag) for the whole group, the male group, and the female group. A one sample *t*-test was used to compute a summary statistic of the distance-sFC(mag) relationship for the whole group ($t(121) = 1.8258$, $p = 0.0703$).

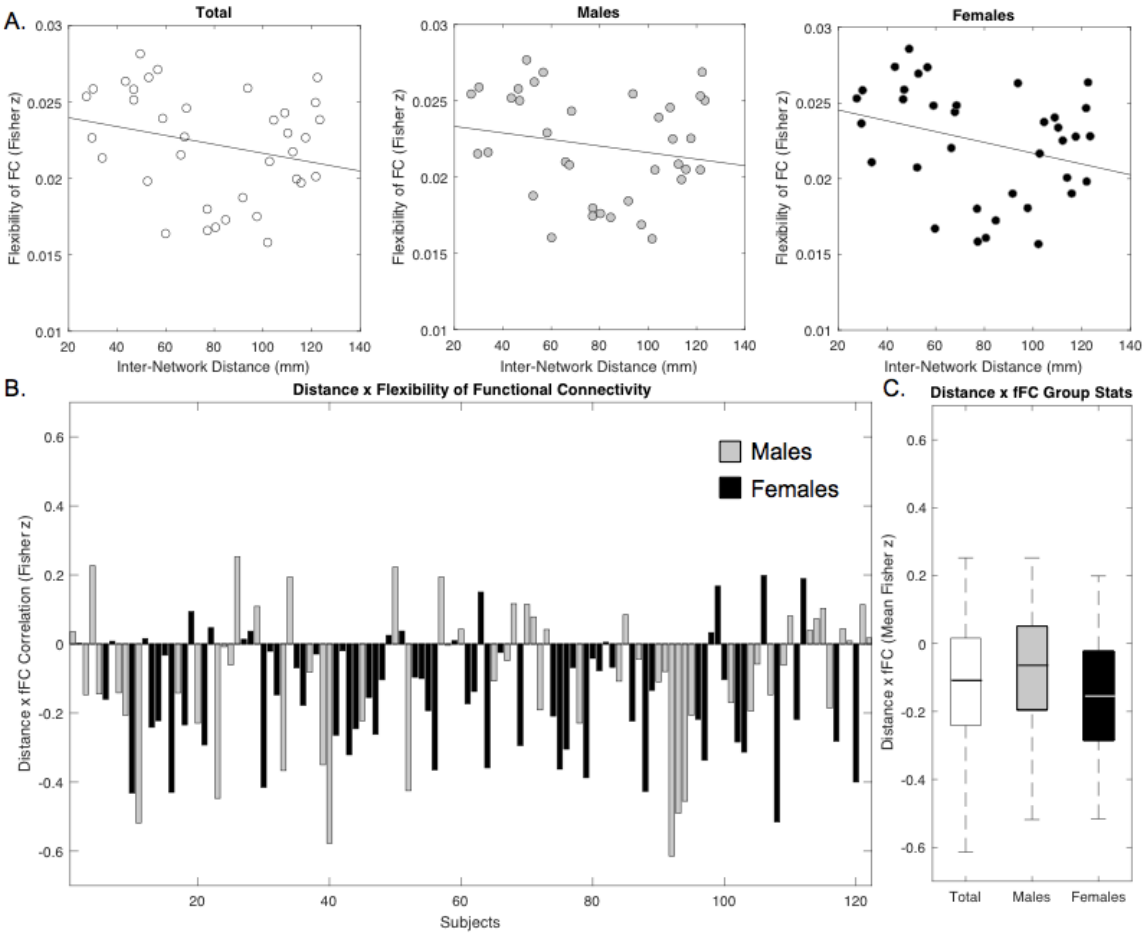

Figure 19. Relationship Between Inter-Network Distance and Flexibility of Functional Connectivity. A. Correlations of distance and fFC averages across subjects are shown for 36 pairs of DMN networks for the whole group ($r(34) = -0.2560$, $p = 0.1319$), the 57 males, and the 65 females. B. Individual within-subject correlations between distance and fFC using 36 pairs of DMN networks are shown. Correlation strengths are presented as Fisher-transformed *z* values. C. The box plots summarize the distributions of the within-subject correlations between distance and fFC for the whole group, the male group, and the female group. A one sample *t*-test was used to compute a summary statistic of the distance-fFC relationship for the whole group ($t(121) = -7.2673$, $p < 0.001$).

Structural and Functional Connectivity

Structural connectivity within the DMN was negatively related to sFC(dir) in the whole group ($t(121) = -7.1118$, $p < 0.001$; Figure 20). Most of the subjects displayed such negative SC-sFC(dir) relationships, although several did show positive correlations. The relationship between SC and sFC(mag), on the other hand, displayed a positive correlation within the entire group (Figure 21), and reached statistical significance ($t(121) = 2.9631$, $p = 0.0037$) despite the lower

summary effect magnitude relative to the SC-sFC(dir) correlation. Individual SC-sFC(mag) correlations did not display the level homogeneity across the entire cohort that was observed across the SC-sFC(dir) correlations, however. Structural connectivity predicted the flexibility of FC in a relatively consistent manner (Figure 22), with positive SC-fFC correlations detected in the majority of study participants, and the summary statistic indicated that the SC-fFC relationship was significant in the entire cohort ($t(121) = 8.6100$, $p < 0.001$).

In addition to the summary *t* statistics, we examined correlations between averaged SC and FC measures to estimate population-level relationships between the two measures. Although we present these findings, caution should be exercised in attempting to infer subject-level SC-FC relationship from the following results. Structural connectivity and sFC(dir) were, on average, not related ($r(34) = 0.1768$, $p = 0.3096$). Likewise, the relationship between SC and sFC(mag) failed to reach statistical significance ($r(34) = 0.0855$, $p = 0.6253$). Averaged SC and fFC, on the other hand, were significantly correlated within the whole group ($r(34) = 0.3464$, $p = 0.0415$).

Given the negative overall SC-sFC(dir) relationship, the repeated measures analysis of variance was conducted in two ways. First, the raw subject-wise SC-sFC(dir) values were used along with the SC-sFC(mag) and SC-fFC values (Table 1). The test, however, did not address our main question of interest regarding which FC measure is related to SC to the greatest degree regardless of the sign. Therefore, a second analogous analysis was conducted in which the signs of the individual subjects' SC-sFC(dir) correlations were flipped, thus

forcing the group summary statistic into the positive direction while preserving the sample variance. This amounted to comparing the magnitudes of SC-sFC(dir), SC-sFC(mag), and SC-fFC relationships (Table 1). The latter test revealed a main effect of SC-FC type ($F(2,242) = 9.082$, $p = 0.001$). The pairwise contrasts indicated significant differences between SC-sFC(dir) and SC-fFC ($MD = 0.049$, $SD = 0.025$, $p = 0.050$) as well as SC-sFC(mag) and SC-fFC ($MD = 0.099$, $SD = 0.016$, $p < 0.001$), with the magnitude of the SC-fFC relationship being greater than both SC-sFC(dir) and SC-sFC(mag). The difference between SC-sFC(dir) and SC-sFC(mag) was not statistically significant ($MD = 0.050$, $SD = 0.027$, $p = 0.070$).

SC-FC Coupling (Raw)

Main Effect	*df*	*F*	*Eta-Squared*	*p*
SC-FC Type	2, 242	*115.045*	0.487	*< 0.001*
Contrasts	*MD*	*St. Dev*	*95% C. I.*	*p*
SC-sFC(dir) vs SC-sFC(mag)	-0.148	0.014	-0.175, -0.121	< 0.001
SC-sFC(dir) vs SC-fFC	-0.247	0.019	-0.284, -0.210	< 0.001
SC-sFC(mag) vs SC-fFC	-0.099	0.016	-0.131, -0.067	< 0.001

SC-FC Coupling (Magnitude)

Main Effect	*df*	*F*	*Eta-Squared*	*p*
SC-FC Type	2, 242	9.082	0.070	0.001
Contrasts	*MD*	*St. Dev*	*95% C. I.*	*p*
SC-sFC(dir) vs SC-sFC(mag)	0.050	0.027	-0.004, 0.104	0.070
SC-sFC(dir) vs SC-fFC	-0.049	0.025	-0.099, 7.927e-5	0.050
SC-sFC(mag) vs SC-fFC	-0.099	0.016	-0.131, -0.067	< 0.001

Table 1. Summary of the Repeated Measures Analysis of Variance of SC-FC Coupling Types. The repeated measures analysis of variance was conducted in two ways: one using the variance from the raw, signed SC-sFC(dir) relationships, and the other with the signs of individual SC-sFC(dir) flipped. The latter analysis was conducted in order to force the SC-sFC(dir) coupling mean in the same direction as SC-sFC(mag) and SC-fFC coupling means while preserving variance, and contrast the structure-function coupling magnitudes.

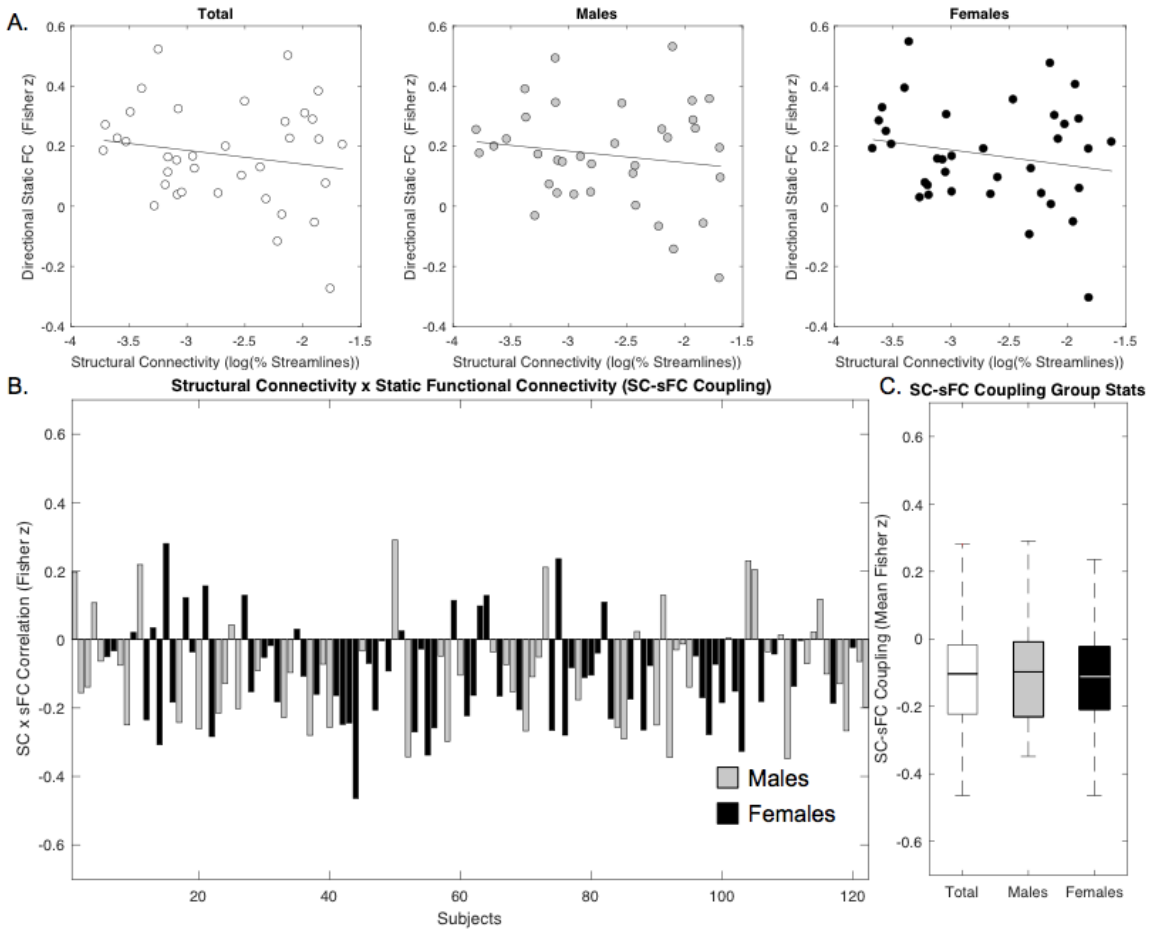

Figure 20. Relationship Between Structural Connectivity and Directional Static Functional Connectivity Across Pairs of Networks Within the Default Mode Network. A. Partial correlations of SC and sFC(dir) averages across subjects, adjusted for mean inter-network Euclidean distances, are shown for 36 pairs of DMN networks for the whole group ($r(34) = 0.1768$, $p = 0.3096$), the 57 males, and the 65 females. B. Individual within-subject partial correlations between SC and sFC(dir), adjusted for inter-network Euclidean distances, using 36 pairs of DMN networks are shown. Correlation strengths are presented as Fisher-transformed *z* values and were corrected for inter-network Euclidean distances. C. The box plots summarize the distributions of the within-subject correlations between SC and sFC(dir) for the whole group, the male group, and the female group. A one sample *t*-test was used to compute a summary statistic of the SC-sFC(dir) relationship for the whole group ($t(121) = -7.1118$, $p < 0.001$).

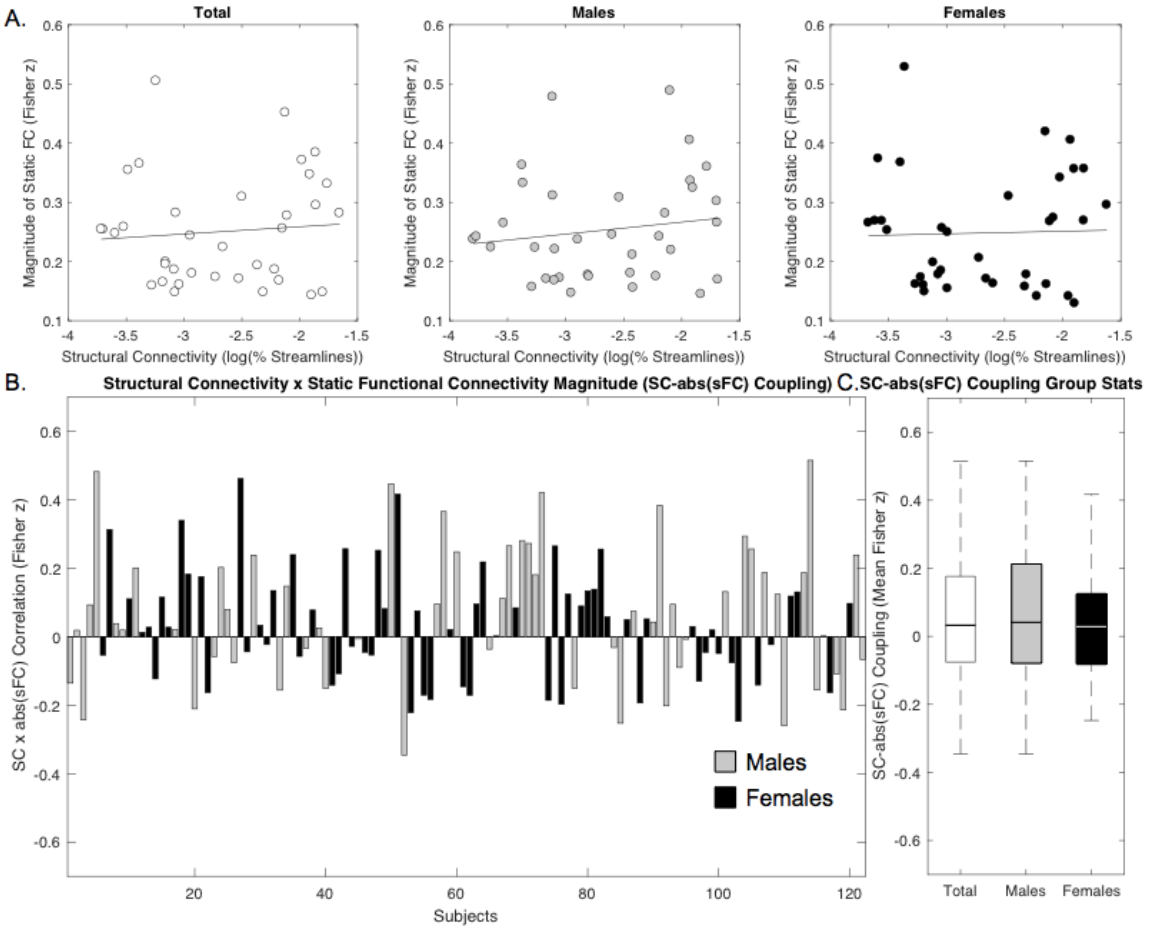

Figure 21. Relationship Between Structural Connectivity and the Magnitude of Static Functional Connectivity Within the Default Mode Network. A. Correlations of SC and abs(sFC), or sFC(mag), averages across subjects are shown for 36 pairs of DMN networks for the whole group ($r(34) = 0.0855$, $p = 0.6253$), the 57 males, and the 65 females. B. Individual within-subject correlations between SC and sFC(mag) using 36 pairs of DMN networks are presented. Correlation strengths are presented as Fisher-transformed *z* values and were corrected for inter-network Euclidean distances. C. The box plots summarize the distributions of the within-subject correlations between SC and sFC(mag) for the whole group, the male group, and the female group. A one sample *t*-test was used to compute a summary statistic of the SC-sFC(mag) relationship for the whole group ($t(121) = 2.9631$, $p = 0.0037$).

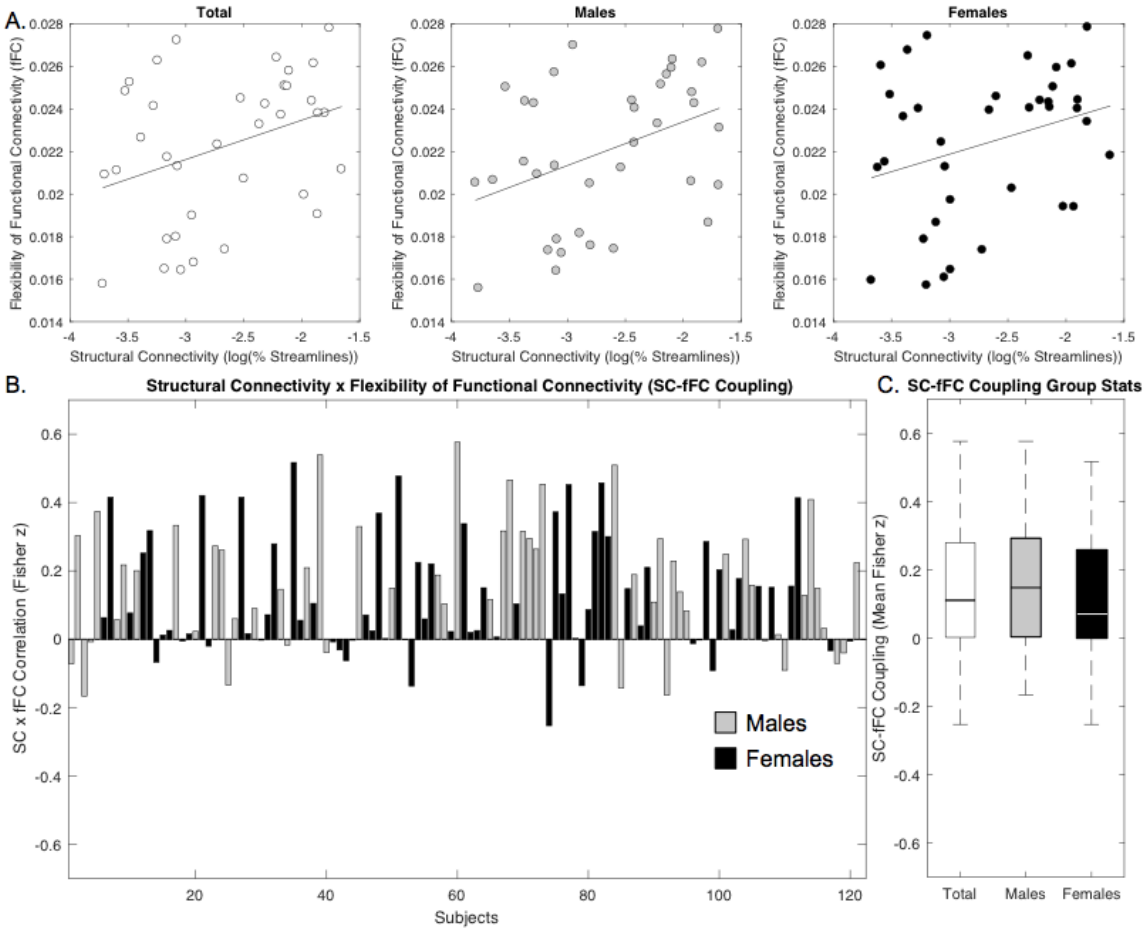

Figure 22. Relationship Between Structural Connectivity and the Flexibility of Functional Connectivity Within the Default Mode Network. A. Correlations of SC and fFC averages across subjects are shown for 36 pairs of DMN networks for the whole group ($r(34) = 0.3464$, $p = 0.0415$), the 57 males, and the 65 females. B. Individual within-subject correlations between SC and fFC using 36 pairs of DMN networks are presented. Correlation strengths are presented as Fisher-transformed *z* values and were corrected for inter-network Euclidean distances. C. The box plots summarize the distributions of the within-subject correlations between SC and fFC for the whole group, the male group, and the female group. A one sample *t*-test was used to compute a summary statistic of the SC-fFC relationship for the whole group ($t(121) = 8.6100$, $p < 0.001$).

Structure-Function Coupling and Individual Differences

The extents to which different types of SC-FC coupling were related to gender, age, and intelligence levels were examined next (Table 2). Directional SC-sFC(dir) was not significantly related to gender ($F(1,116) = 0.296$, $p = 0.588$), age ($F(1,116) = 1.497$, $p = 0.224$), or IQ ($F(1,116) = 0.603$, $p = 0.439$). The gender x age ($F(1,116) = 0.932$, $p = 0.336$) and gender x IQ ($F(1,116) = 0.640$, $p = 0.425$) interactions did not reach statistical significance. Figure 23 summarizes

the relationships between the behavioral measures and SC-sFC(dir) via partial correlation across gender. Analogously, SC-sFC(mag) was also not related to gender ($F(1,116) = 0.074$, $p = 0.786$), age ($F(1,116) = 0.886$, $p = 0.349$), or IQ ($F(1,116) = 0.852$, $p = 0.358$). The gender x age ($F(1,116) = 0.564$, $p = 0.454$) and gender x IQ ($F(1,116) = 0.656$, $p = 0.420$) interactions were not significant either. Figure 24 summarizes the findings via partial correlations across gender. The SC-fFC measure was not related to gender ($F(1,116) = 0.836$, $p = 0.362$) or age ($F(1,116) = 0.819$, $p = 0.367$), but a significant effect of IQ was observed ($F(1,116) = 3.932$, $p = 0.050$). Neither the gender x age ($F(1,116) = 0.359$, $p = 0.550$) or the gender x IQ interactions ($F(1,116) = 0.463$, $p = 0.498$), however, reached statistical significance. The results are summarized via partial correlations across gender in Figure 25.

SC-FC Type	*Effect/Interaction*	*df*	*F*	*Eta-Squared*	*p*
SC-sFC(dir)	Gender	1, 116	0.296	0.003	0.588
	Age	1, 116	1.497	0.013	0.224
	IQ	1, 116	0.603	0.005	0.439
	Gender x Age	1, 116	0.932	0.008	0.336
	Gender x IQ	1, 116	0.640	0.005	0.425
SC-sFC(mag)	Gender	1, 116	0.074	0.001	0.786
	Age	1, 116	0.886	0.008	0.349
	IQ	1, 116	0.852	0.007	0.358
	Gender x Age	1, 116	0.564	0.005	0.454
	Gender x IQ	1, 116	0.656	0.006	0.420
SC-fFC	Gender	1, 116	0.836	0.007	0.362
	Age	1, 116	0.819	0.007	0.367
	IQ	1, 116	3.932	0.033	0.050
	Gender x Age	1, 116	0.359	0.003	0.550
	Gender x IQ	1, 116	0.463	0.004	0.498

Table 2. Relationship Between Behavioral Measures and Different Types of SC-FC Coupling. Multivariate analysis of variance results are summarized for the relationships between gender, age, and iq and SC-sFC(dir), SC-sFC(mag), and SC-fFC coupling types.

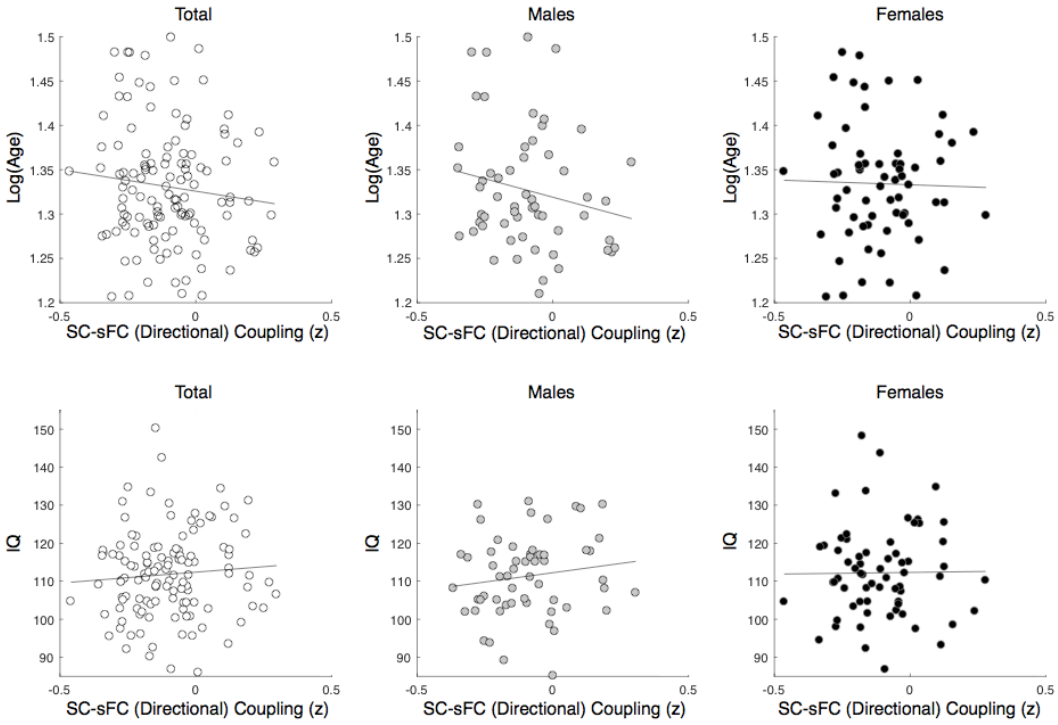

Figure 23. SC-sFC(dir) Coupling, Age, and IQ. Top panel: correlations between SC-sFC(dir) coupling and age are presented for the entire study sample, the male group, and the female group. Bottom panel: partial correlations between SC-sFC(dir) coupling and IQ, adjusted for age, are shown for the total sample, the male group, and the female group.

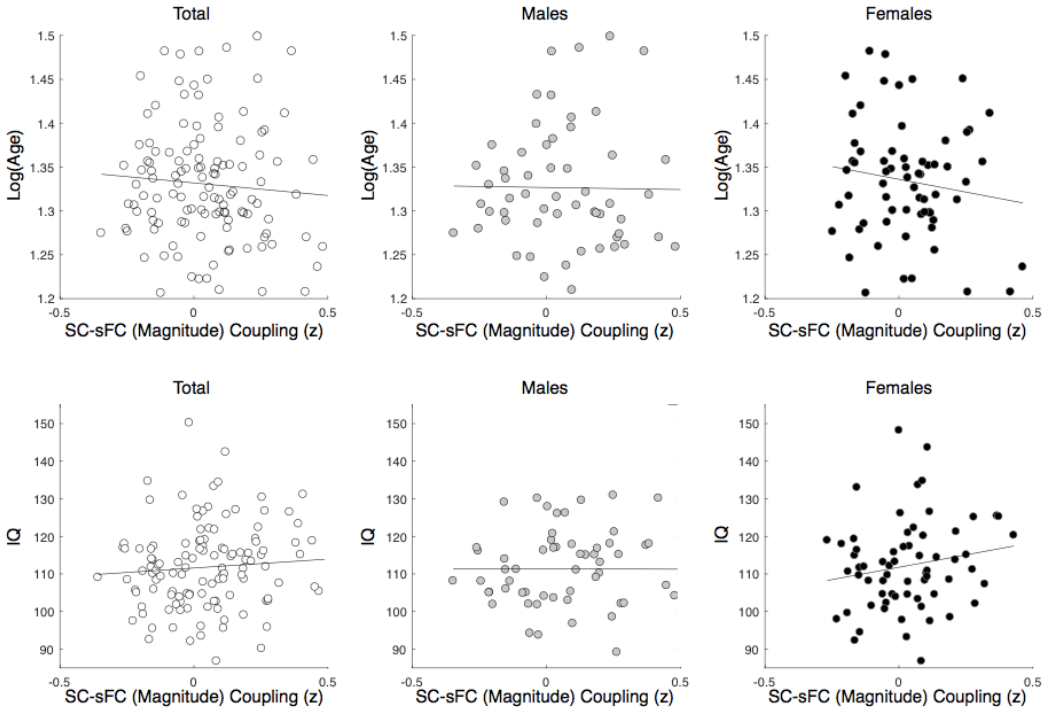

Figure 24. SC-sFC(mag) Coupling, Age, and IQ. Top panel: correlations between SC-sFC(mag) coupling and age are presented for the entire study sample, the male group, and the female group. Bottom panel: Age-adjusted partial correlations between SC-sFC(mag) coupling and IQ are shown for the total sample, the male group, and the female group.

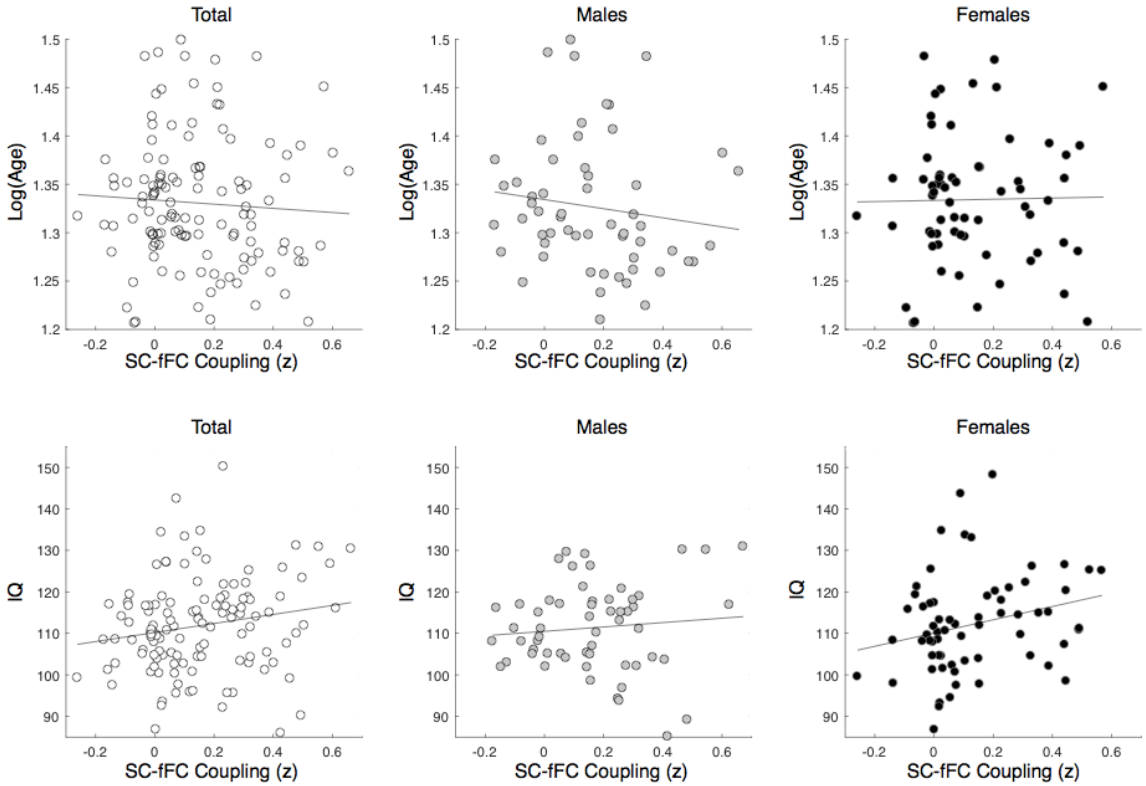

Figure 25. SC-fFC Coupling, Age, and IQ. Top panel: correlations between SC-fFC coupling and age are presented for the entire study sample, the male group, and the female group. Bottom panel: partial correlations between SC-fFC coupling and IQ, adjusted for age, are shown for the total sample, the male group, and the female group.

CHAPTER 4: DISCUSSION

Main Findings

Using fMRI data obtained from a moderately sized sample, we showed that the flexibilities of between-network connectivity levels within the DMN are related to the strengths of the structural connections that underlie them. Networks pairs with stronger white matter connections between them tended to exercise more variable levels of functional connectivity. Further, we detected that this relationship between structural connectivity (SC) and the flexibility of functional connectivity (fFC), or SC-fFC coupling, was positively related to intelligence levels. Specifically, stronger SC-fFC coupling levels were associated

with higher IQ scores. This is suggestive of a positive relationship between structure-function efficiency within the DMN and cognitive ability.

Structure and Static Connectivity

The observed relationship between structural and raw directional static functional connectivity levels within the DMN was unexpected and inconsistent with other analyses that have examined SC-sFC correspondences across the whole brain. Specifically, we detected a negative SC-sFC(dir) relationship, while others have reported strong positive associations between the two variables (Hagmann et al. 2008; Skudlarski et al. 2008; Honey et al. 2009). Given that we did not examine the whole brain, it is difficult to draw conclusions about this discrepancy, as the SC-sFC(dir) relationship within the DMN may in fact be negative. Recent findings have suggested that within-DMN functional patterns may be more heterogeneous than previously thought (Chen et al. 2017). The system-specific structure-function relationship within the DMN described herein may therefore not be reflective of the patterns across the entire brain or other systems.

Another compelling argument for the unexpected result pertains to the treatment of anti-correlations in task-free fMRI data. Figure 20-A elucidates the nature of the negative SC-sFC relationship, showing three network pairs with strong negative FC (anti-correlations) in the top quartile of the SC distribution, which in turn likely drove the slope of the correlation down. The subsequent analysis of the relationship between SC and sFC(mag) did, however, show a

significant positive correlation (Figure 21). Collectively, these results convey that the general relationship between SC and sFC is consistent across both anti-correlated and positively correlated network pairs. Specifically, SC increases with strengthened positive sFC across network pairs. Likewise, SC increases as negative sFC levels become stronger, or more anti-correlated, as well. Previous reports, however, are not suggestive of this pattern, showing ROI pairs with highly positive sFC having very strong SC levels, yet those with highly anti-correlated sFC possessing very weak SC (Honey et al. 2009). Such results convey that the SC-sFC relationship is inconsistent, perhaps even inversed, across region pairs that display positive and negative sFC levels. Given the existing reports' use of very large numbers of ROIs that were derived anatomically, the dilemma described above may have failed to come to light due to the fact that the vast majority of ROI pairs exhibited positive sFC, as was the case in our data as well. We are therefore reluctant to draw further inferences from the SC-sFC(dir) analysis, and instead highlight that the observed SC-sFC(mag) coupling, while positive, was relatively weak – an unexpected result in the light of strong positive whole-brain structure-function relationships reported by other groups.

In addressing the unexpected SC-sFC(mag) relationship within the DMN, we emphasize that, in contrast to the anatomically-defined ROIs used in prior SC-sFC investigations, the present study used ICA-derived functional networks. This approach was fundamentally more advantageous, as it yielded networks that were maximally functionally independent from each other, and parsed out

redundant signal that would have contaminated any pair of small ROIs in seed-based sFC analyses, particularly ones that are in proximity of each other. Raw BOLD activity levels in a particular voxel inevitably contain information about multiple simultaneous processes, and such signals cannot be considered to be uniquely representing any single brain region. This is effectively addressed by ICA, which decomposes each voxel's aggregate activity into contributions to multiple ongoing processes in the brain. Inter-regional FC obtained from the resulting ICA-derived time courses thus effectively excludes contamination from other processes, which are left in seed-based FC measures.

Further, we reiterate that, to our knowledge, the fMRI temporal resolution and the number of DWI gradient directions used in the present study superseded those utilized by all other structure-function investigations to date. Given the relatively high temporal resolution (TR = 0.275 ms) of our fMRI data and 150-directional DWI sequence, coupled with a post-processing methodology that yields regional signals of high fidelity, we argue that the within-DMN SC-sFC(mag) coupling during task-free scans may in fact be weaker than previously thought. The results from the decomposition of sFC into recurring FC states via clustering, discussed below, provides further insight into the reasons why this may be the case.

Structure and Flexibility of Functional Connectivity

Structural connectivity and the flexibility of functional connectivity displayed a strong positive relationship (Figure 22). Interestingly, the examination

of specific FC states provides insight into what was actually measured in the case of task-free sFC. Let us first acknowledge that the six isolated clusters used for the fFC analysis are derivatives of sFC, meaning that averaging across the FC states would approximate the aggregate sFC. In considering FC state 4 (Figure 12), it is apparent that none of the networks exhibited substantial functional connectivity levels among them, thus forming a state of DMN-wide disconnectedness. Additionally, this particular state was occupied for nearly half of the entire scan time across subjects, meaning that the presence of this state in the data would substantially bias the observed sFC toward zero. This may account for the relatively weak relationship between structure and static functional connectivity that we reported.

The DMN has been shown to reflect the structural and functional core of the human brain (Hagmann et al. 2008), with the ability to integrate information from other regions. We must not forget that task-free state scans do not provide much information for this core to operate upon. The nature of state 4 therefore provides compelling evidence that, during task-free scans, the DMN may not be utilized to its full potential in information integration. Static FC would thus be contaminated with such state of disconnectedness throughout the scan. This brings into question the power of task-free sFC to be extrapolated to other scenarios. In other words, task-free sFC may be quantifying what the brain is doing in the absence of cognitive engagement, and may not accurately reflect its potential capabilities under other, real-world situations.

Another explanation for the prominence and nature of state 4 may lie in the possibility that it reflects state-to-state transitional processes. As networks shift from one pattern of connectivity to another, they become functionally disconnected and deviate from the FC states detected via clustering, crossing the FC of zero as they alternate between being positively and negatively correlated. Given that such shifts likely occur at rates that are much more rapid than ones detectable with fMRI, which has relatively low temporal resolution, state 4 may be produced by periods of high-rate state-to-state shifts. If true, this particular state would be considered a mathematical artifact rather than stable periods of true disconnectedness within the DMN. Future studies could investigate this question by examining the time courses of state transitions. An application of graph theory to such data, for example, could determine whether state 4 acts as an intermediate transitional hub, which other states pass through as they shift between each other.

In contrast to sFC measures, the fFC measure we proposed captures the variability of connectivity patterns that the brain exhibits in a task-free setting, and therefore may be more reflective of what the brain is capable of under other conditions. This is supported by the robust positive relationship between SC and fFC that we described. Taken collectively with the relatively weak link between SC and sFC, the findings are suggestive of the fact that brain structure is simply not designed to facilitate a state of cognitive disengagement, but rather to support the integration of cognition and rapidly incoming real-world information. Supporting this argument is the fact that the SC-sFC relationship was not

predictive of our behavioral measure, but the SC-fFC link was, which is discussed below.

SC-FC Coupling, Gender, Age, and IQ

The SC-sFC(dir) and SC-sFC(mag) measures were not related to age, intelligence levels, or gender, and SC-fFC coupling was not related to age or gender. Previous examinations of DMN connectivity have described substantial developmental effects on functional connectivity in children (Fair et al. 2008). Further, different region pairs may undergo non-parallel changes in terms of structural and functional connectivity. The link between prefrontal cortices and the posterior cingulate cortex, for example, appeared to be weak both structurally and functionally in young children and strengthening as a function of age. However, children displayed functional connectivity between the middle temporal lobe and the posterior cingulate cortex that was similar to that in adults, even though the structural connection between these regions was largely underdeveloped (Supekar et al. 2010). Despite such developmental effects in school-aged children, the lack of age effects on any of the three SC-FC relationship types in our analysis suggests that during young adulthood, the DMN system may exist in a relatively homeostatic state, with any ongoing changes in SC and sFC occurring in parallel. However, given the narrow age range of the analyzed cohort, we caution against making any inferences pertaining to the effects of age on SC-sFC coupling based on our null findings.

Intelligence levels did display a significant relationship with SC-fFC coupling. Specifically, IQ appeared to increase as the functional connections within the DMN were afforded more variance by the stronger underlying structure. Importantly, IQ was not related to either type of SC-sFC coupling, strengthening our argument that task-free sFC may be underpowered in providing insight into functional brain correlates of behaviors outside of the scanner. Further, the novel fFC measure may be reflective of white matter efficiency, which has been demonstrated to have a positive relationship with cognitive ability (van den Heuvel et al. 2009). In other words, the structural efficiency of pathways that the brain relies on to integrate information from other regions is predictive of intelligence levels. This relationship has additionally been shown to differ between genders. Global white matter efficiency was found to be predictive of cognitive ability in females, but no such relationship was detected in males (Ryman et al. 2016). Specifically, while females appeared to benefit from more direct white matter connections across the brain, males did not rely on them to achieve similar intelligence levels. However, we did not detect a significant interaction between gender and IQ in their influences on SC-fFC, raising the possibility that the gender discrepancy in the relationship between white matter efficiency and intelligence may not be homogeneous across different brain systems, such as the DMN. Previous findings suggesting that overall white matter efficiency is related to intelligence levels support the notion that structure is built to facilitate states of cognitive engagement rather than task-free settings. The fact that the SC-fFC relationship is predictive of IQ, but the SC-

sFC is not, demonstrates the extrapolative power that fFC holds over sFC for future analyses attempting to relate task-free functional connectivity to behavioral measures.

On Global Signal and Anti-Correlations

Functional connectivity state 4 has the potential to reflect global signal. However, we argue here that this is an unlikely possibility given the methodology employed, and that it may represent a true state of disconnectedness within the DMN. Also discussed is the fact that previously published examinations of the SC-FC relationship treated anti-correlations with skepticism, classifying them as potential artifacts, and went as far as exclude them from the investigations. However, we argue that anti-correlations present in the described data are genuine, and were legitimately retained in the conducted analysis.

This scrutiny of anti-correlations was warranted by the possibility of their artificial introductions via certain processing techniques. Specifically, the removal of global BOLD signal mean, which is defined as artifact-based signal that spans the entire brain, has been implicated in producing spurious anti-correlations in fMRI data (Fox et al. 2009; Murphy et al. 2009; Carbonell et al. 2011; Power et al. 2017). In contrast to GLM-based approaches that utilize contrasts, which effectively blind them to global effects, task-free data analyses rely on the spatiotemporal structures that are present in the data, and are thus sensitive to any potential global contaminants. Removing such signals is therefore a crucial pre-processing step in any attempt to investigate task-free brain activity. Global

signal regression is a common approach to doing so, particularly in the case of seed-based network extraction. However, if two positively correlated voxels with time courses A and B are regressed onto global signal C, the two resulting sets of residuals have the potential to be anti-correlated, particularly as vector C approaches the mean of vectors A and B. Such spurious anti-correlations have been shown to contaminate task-free data when global signal regression is utilized in seed-based approaches to quantifying fMRI FC (Murphy et al. 2009).

The DMN has been of special interest in investigating potential spurious anti-correlations given that its defining feature is increased activity in the absence of a task, which decreases once the brain becomes cognitively engaged (Greicius et al. 2003). This attribute of the DMN has earned it the classification of a task-negative network, which stands in contrast to task-positive networks, which become activated when the brain is subjected to cognitive load. The DMN is therefore anti-correlated with task-positive networks, and the consistent initial descriptions of this relationship have been suggested to be due to global mean removal. The network has stood up to the test of time, however, having been isolated using multiple network extraction techniques, and displaying robust anti-correlations with task-positive networks, as well as within itself (Long et al. 2008; Allen et al. 2011; Chen et al. 2017).

Although seed-based task-free analyses carry the risk of detecting spurious anti-correlations via global mean regression, the network extraction methodology employed in the present study addresses global effects in a manner that is less susceptible to artifact introduction. With global BOLD signal never

explicitly regressed, we used PCA preprocessing coupled with ICA decomposition, which implicitly remove such global effects. Specifically, PCA was used to whiten the data prior to ICA, which yielded a mean global component that was subsequently removed from the data at each time point. Given the orthogonality that PCA imposes on the isolated principal components (PCs), the removed PC did not contribute to any other networks that were left in the data. This effectively removed the global mean without affecting data in networks of interest. Indeed, it has been demonstrated that task-free global activity, as derived by PCA, is uncorrelated to other brain-based networks, and may serve as a useful tool for removal of artifact-based signal without adulterating brain-based BOLD fluctuations (Carbonell et al. 2011). In addition to PCA preprocessing, ICA has also been suggested to be an effective way to circumvent global signal regression by excluding components deemed to represent noise and artifacts (Fox et al. 2009). Considering the methodology we employed, the anti-correlations in our data are likely to be genuine DMN processes, and were retained in the SC-sFC analysis.

Other Limitations

Given the bivariate nature of the analysis, it is yet to be determined whether stronger SC results in increased flexibility of FC, or vice versa. Analogous analyses in children and adolescent populations may elaborate on this question in future studies, however. Additionally, subsequent studies should attempt to extrapolate the findings presented here to the whole brain, as within-

DMN connectivity relationships between structure and functional flexibility may not be reflective of other cognitive systems. Examining this relationship in the connections between the DMN and other networks would be of particular interest, since the DMN is known to fluctuate substantially in its FC to other networks as the brain switches from a task-free state to cognitive engagement.

We note that modularity was not considered in the present analysis, focusing instead on direct tractography-based inter-network connections. It has been demonstrated that separate regions can in fact display synchronous activity levels in the absence of direct white matter projections (Greicius et al. 2009) – medial prefrontal cortex (MPFC) and middle temporal gyri in particular, which implies the involvement of other brain regions. While our ICA-based approach did not isolate MPFC proper as part of the DMN, the anterior cingulate and middle frontal gyri did show connections to other DMN networks. Nevertheless, it is a near-certain reality that intermediate regions, such as the thalamus, contribute to the synchronies exhibited by spatially separate network pairs. Although graph theoretical analyses have considered such interactions, the areas considered have so far been anatomically defined. As such, it would be of interest to examine the connections between functionally-defined networks using graph theory in future investigations.

CHAPTER 5: CONCLUSIONS

We proposed a novel measure of dynamic functional network connectivity (FNC) using flexibility of functional connectivity (fFC), which captures the variance of functional connectivity across time. The novel measure was demonstrated to quantitatively reflect the underlying structural connectivity within the default mode network, while static functional connectivity (sFC) did so to a relatively low and inconsistent degree. As SC likely does not develop to facilitate brain function in task-free settings, but rather to integrate information during cognitive engagement, we argue that fFC can estimate the potential functional connectivity exhibited outside of the resting state to a greater degree than sFC, and is better suited for examining behavioral correlates of FNC. Supporting this notion, we showed that SC-fFC coupling was related to intelligence levels, while SC-sFC coupling was not. Further, we found that the DMN existed in a functionally disconnected state during a large portion of the resting scan, raising questions about whether sFC is a meaningful quantifier of functional connectivity in the absence of a task, and scrutinizing its extrapolative power to real-world, cognitively engaging scenarios. While the question of whether this state of disconnectedness reflects biological processes or is an artifact remains, fFC is based on FNC variability across time rather than its average, and is largely unaffected by such contaminants during rest.

REFERENCES

Aggarwal CC, Hinneburg A, Keim DA. 2001. On the Surprising Behavior of Distance Metrics in High Dimensional Space. In: Lecture Notes in Computer Science. Springer. p. 420–434.

Allen EA, Damaraju E, Plis SM, Erhardt EB, Eichele T, Calhoun VD. 2012. Tracking Whole-Brain Connectivity Dynamics in the Resting State. Cereb Cortex.

Allen EA, Erhardt EB, Damaraju E, Gruner W, Segall JM, Silva RF, Havlicek M, Rachakonda S, Fries J, Kalyanam R, Michael AM, Caprihan A, Turner JA, Eichele T, Adelsheim S, Bryan AD, Bustillo J, Clark VP, Feldstein Ewing SW, Filbey F, Ford CC, Hutchison K, Jung RE, Kiehl KA, Kodituwakku P, Komesu YM, Mayer AR, Pearlson GD, Phillips JP, Sadek JR, Stevens M, Teuscher U, Thoma RJ, Calhoun VD. 2011. A Baseline for the Multivariate Comparison of Resting-State Networks. Front Syst Neurosci. 5.

Behrens TEJ, Berg HJ, Jbabdi S, Rushworth MFS, Woolrich MW. 2007. Probabilistic diffusion tractography with multiple fibre orientations: What can we gain? Neuroimage. 34:144–155.

Biswal B, Zerrin Yetkin F, Haughton VM, Hyde JS. 1995. Functional connectivity in the motor cortex of resting human brain using echo-planar mri. Magnetic Resonance in Medicine. 34:537–541.

Brookes MJ, Hale JR, Zumer JM, Stevenson CM, Francis ST, Barnes GR, Owen JP, Morris PG, Nagarajan SS. 2011. Measuring functional connectivity

using MEG: Methodology and comparison with fcMRI. Neuroimage. 56:1082–1104.

Calhoun V, Adali T, Pearlson G. 2001. Independent component analysis applied to fMRI data: a generative model for validating results. In: Neural Networks for Signal Processing XI, 2001. Proceedings of the 2001 IEEE Signal Processing Society Workshop. Presented at the Neural Networks for Signal Processing XI, 2001. Proceedings of the 2001 IEEE Signal Processing Society Workshop. p. 509–518.

Calhoun VD, Adali T. 2006. Unmixing fMRI with independent component analysis. IEEE Engineering in Medicine and Biology Magazine. 25:79–90.

Carbonell F, Bellec P, Shmuel A. 2011. Global and System-Specific Resting-State fMRI Fluctuations Are Uncorrelated: Principal Component Analysis Reveals Anti-Correlated Networks. Brain Connect. 1:496–510.

Chen JE, Glover GH, Greicius MD, Chang C. 2017. Dissociated patterns of anti-correlations with dorsal and ventral default-mode networks at rest. Hum Brain Mapp. n/a-n/a.

Comon P. 1994. Higher Order StatisticsIndependent component analysis, A new concept? Signal Processing. 36:287–314.

Correa N, Adali T, Calhoun VD. 2007. Performance of Blind Source Separation Algorithms for FMRI Analysis using a Group ICA Method. Magn Reson Imaging. 25:684–694.

Correa N, Adali T, Li Y-O, Calhoun VD. 2005. Comparison of blind source separation algorithms for FMRI using a new Matlab toolbox: GIFT. In:

Proceedings. (ICASSP ’05). IEEE International Conference on Acoustics, Speech, and Signal Processing, 2005. Presented at the Proceedings. (ICASSP ’05). IEEE International Conference on Acoustics, Speech, and Signal Processing, 2005. p. v/401-v/404 Vol. 5.

Delorme A, Plamer R, Oostenveld R, Onton J, Makeig S. 2007. Comparing results of algorithms implementing blind source separation of EEG data. Swartz Foundation and NIH Grant.

Dodel S, Herrmann M, Geisel T. 2000. Comparison of temporal and spatial ica in fmri data analysis. Proceedings of ICA2000, the Second International Conference on Independent Component Analysis and Signal Separation.

Douek P, Turner R, Pekar J, Patronas N, Le Bihan D. 1991. MR color mapping of myelin fiber orientation. J Comput Assist Tomogr. 15:923–929.

Fair DA, Cohen AL, Dosenbach NUF, Church JA, Miezin FM, Barch DM, Raichle ME, Petersen SE, Schlaggar BL. 2008. The maturing architecture of the brain’s default network. PNAS. 105:4028–4032.

Fomina T, Hohmann M, Scholkopf B, Grosse-Wentrup M. 2015. Identification of the Default Mode Network with electroencephalography. Conf Proc IEEE Eng Med Biol Soc. 2015:7566–7569.

Fox MD, Snyder AZ, Vincent JL, Corbetta M, Essen DCV, Raichle ME. 2005. The human brain is intrinsically organized into dynamic, anticorrelated functional networks. PNAS. 102:9673–9678.

Fox MD, Zhang D, Snyder AZ, Raichle ME. 2009. The Global Signal and Observed Anticorrelated Resting State Brain Networks. Journal of Neurophysiology. 101:3270–3283.

Gozzi A, Schwarz AJ. 2016. Large-scale functional connectivity networks in the rodent brain. Neuroimage. 127:496–509.

Greicius MD, Krasnow B, Reiss AL, Menon V. 2003. Functional connectivity in the resting brain: A network analysis of the default mode hypothesis. PNAS. 100:253–258.

Greicius MD, Supekar K, Menon V, Dougherty RF. 2009. Resting-State Functional Connectivity Reflects Structural Connectivity in the Default Mode Network. Cerebral cortex (New York, NY : 1991). 19:72.

Hagmann P, Cammoun L, Gigandet X, Meuli R, Honey CJ, Wedeen VJ, Sporns O. 2008. Mapping the Structural Core of Human Cerebral Cortex. PLOS Biology. 6:e159.

Honey CJ, Sporns O, Cammoun L, Gigandet X, Thiran JP, Meuli R, Hagmann P. 2009. Predicting human resting-state functional connectivity from structural connectivity. PNAS. 106:2035–2040.

Joel SE, Caffo BS, van Zijl PC, Pekar JJ. 2011. On the relationship between seed-based and ICA-based measures of functional connectivity. Magn Reson Med. 66:644–657.

Jutten C, Herault J. 1991. Blind separation of sources, part I: An adaptive algorithm based on neuromimetic architecture. Signal Processing. 24:1–10.

Karapanagiotidis T, Bernhardt BC, Jefferies E, Smallwood J. 2016. Tracking thoughts: Exploring the neural architecture of mental time travel during mind-wandering. Neuroimage. 147:272–281.

Knyazev GG, Savostyanov AN, Bocharov AV, Tamozhnikov SS, Saprigyn AE. 2016. Task-positive and task-negative networks and their relation to depression: EEG beamformer analysis. Behav Brain Res. 306:160–169.

Kobayashi Y, Amaral DG. 2003. Macaque monkey retrosplenial cortex: II. Cortical afferents. J Comp Neurol. 466:48–79.

Kucyi A, Esterman M, Riley CS, Valera EM. 2016. Spontaneous default network activity reflects behavioral variability independent of mind-wandering. Proc Natl Acad Sci USA. 113:13899–13904.

Kyathanahally SP, Jia H, Pustovyy OM, Waggoner P, Beyers R, Schumacher J, Barrett J, Morrison EE, Salibi N, Denney TS, Vodyanoy VJ, Deshpande G. 2015. Anterior-posterior dissociation of the default mode network in dogs. Brain Struct Funct. 220:1063–1076.

Lavenex P, Suzuki WA, Amaral DG. 2002. Perirhinal and parahippocampal cortices of the macaque monkey: projections to the neocortex. J Comp Neurol. 447:394–420.

Lee RF. 2015. Emergence of the default-mode network from resting-state to activation-state in reciprocal social interaction via eye contact. Conf Proc IEEE Eng Med Biol Soc. 2015:1821–1824.

Lloyd S. 1982. Least squares quantization in PCM. IEEE Transactions on Information Theory. 28:129–137.

Long X-Y, Zuo X-N, Kiviniemi V, Yang Y, Zou Q-H, Zhu C-Z, Jiang T-Z, Yang H, Gong Q-Y, Wang L, Li K-C, Xie S, Zang Y-F. 2008. Default mode network as revealed with multiple methods for resting-state functional MRI analysis. Journal of Neuroscience Methods. 171:349–355.

Lu H. 2012. Rat brains also have a default mode network. Rat brains also have a default mode network. 109:3979–3984.

Mantini D, Gerits A, Nelissen K, Durand J-B, Joly O, Simone L, Sawamura H, Wardak C, Orban GA, Buckner RL, Vanduffel W. 2011. Default Mode of Brain Function in Monkeys. J Neurosci. 31:12954–12962.

Mazoyer B, Zago L, Mellet E, Bricogne S, Etard O, Houdé O, Crivello F, Joliot M, Petit L, Tzourio-Mazoyer N. 2001. Cortical networks for working memory and executive functions sustain the conscious resting state in man. Brain Research Bulletin. 54:287–298.

McKeown MJ, Sejnowski TJ. 1998. Independent component analysis of fMRI data: examining the assumptions. Hum Brain Mapp. 6:368–372.

Mori S, Crain BJ, Chacko VP, van Zijl PC. 1999. Three-dimensional tracking of axonal projections in the brain by magnetic resonance imaging. Ann Neurol. 45:265–269.

Murphy K, Birn RM, Handwerker DA, Jones TB, Bandettini PA. 2009. The impact of global signal regression on resting state correlations: Are anti-correlated networks introduced? NeuroImage. 44:893–905.

Power JD, Plitt M, Laumann TO, Martin A. 2017. Sources and implications of whole-brain fMRI signals in humans. NeuroImage. 146:609–625.

Qin P, Grimm S, Duncan NW, Fan Y, Huang Z, Lane T, Weng X, Bajbouj M, Northoff G. 2016. Spontaneous activity in default-mode network predicts ascription of self-relatedness to stimuli. Soc Cogn Affect Neurosci. 11:693–702.

Raichle ME, MacLeod AM, Snyder AZ, Powers WJ, Gusnard DA, Shulman GL. 2001. A default mode of brain function. PNAS. 98:676–682.

Robinson JL, Baxi M, Katz JS, Waggoner P, Beyers R, Morrison E, Salibi N, Denney TS, Vodyanoy V, Deshpande G. 2016. Characterization of Structural Connectivity of the Default Mode Network in Dogs using Diffusion Tensor Imaging. Sci Rep. 6:36851.

Ryman SG, Yeo RA, Witkiewitz K, Vakhtin AA, van den Heuvel M, de Reus M, Flores RA, Wertz CR, Jung RE. 2016. Fronto-Parietal gray matter and white matter efficiency differentially predict intelligence in males and females. Hum Brain Mapp. n/a-n/a.

Shannon CE. 1949. Communication in the Presence of Noise. Proceedings of the IRE. 37:10–21.

Shulman GL, Fiez JA, Corbetta M, Buckner RL, Miezin FM, Raichle ME, Petersen SE. 1997. Common Blood Flow Changes across Visual Tasks: II. Decreases in Cerebral Cortex. J Cogn Neurosci. 9:648–663.

Skudlarski P, Jagannathan K, Calhoun VD, Hampson M, Skudlarska BA, Pearlson G. 2008. Measuring brain connectivity: diffusion tensor imaging validates resting state temporal correlations. Neuroimage. 43:554–561.

Soch J, Deserno L, Assmann A, Barman A, Walter H, Richardson-Klavehn A, Schott BH. 2016. Inhibition of Information Flow to the Default Mode Network During Self-Reference Versus Reference to Others. Cereb Cortex.

Sporns O, Chialvo DR, Kaiser M, Hilgetag CC. 2004. Organization, development and function of complex brain networks. Trends in Cognitive Sciences. 8:418–425.

Stejskal EO, Tanner JE. 1965. Spin Diffusion Measurements: Spin Echoes in the Presence of a Time‐Dependent Field Gradient. The Journal of Chemical Physics. 42:288–292.

Supekar K, Uddin LQ, Prater K, Amin H, Greicius MD, Menon V. 2010. Development of functional and structural connectivity within the default mode network in young children. NeuroImage. 52:290–301.

van den Heuvel MP, Hulshoff Pol HE. 2010. Exploring the brain network: A review on resting-state fMRI functional connectivity. European Neuropsychopharmacology. 20:519–534.

van den Heuvel MP, Stam CJ, Kahn RS, Hulshoff Pol HE. 2009. Efficiency of functional brain networks and intellectual performance. J Neurosci. 29:7619–7624.

Van Dijk KRA, Hedden T, Venkataraman A, Evans KC, Lazar SW, Buckner RL. 2010. Intrinsic functional connectivity as a tool for human connectomics: theory, properties, and optimization. J Neurophysiol. 103:297–321.

Weinstein D, Kindlmann G, Lundberg E. 1999. Tensorlines: advection-diffusion based propagation through diffusion tensor fields. In: Visualization ’99. Proceedings. Presented at the Visualization ’99. Proceedings. p. 249–530.

Xi J, Chicharo JF, Tsoi AC, Siu W-C. 2000. On the INFOMAX algorithm for blind signal separation. In: 5th International Conference on Signal Processing Proceedings, 2000. WCCC-ICSP 2000. Presented at the 5th International Conference on Signal Processing Proceedings, 2000. WCCC-ICSP 2000. p. 425–428 vol.1.

Xu X, Yuan H, Lei X. 2016. Activation and Connectivity within the Default Mode Network Contribute Independently to Future-Oriented Thought. Sci Rep. 6:21001.